AD-A269 206

ARMY RESEARCH LABORATORY

Aerodynamic Characteristics of a Helicopter Rotor Airfoil as Affected by Simulated Ballistic Damage

J. Gordon Leishman

ARL-CR-66   September 1993

DTIC
ELECTE
SEP 14 1993
S   D
A

93 9 13 010

93-21214

NOTICES

Destroy this report when it is no longer needed. DO NOT return it to the originator.

Additional copies of this report may be obtained from the National Technical Information Service, U.S. Department of Commerce, 5285 Port Royal Road, Springfield, VA 22161.

The findings of this report are not to be construed as an official Department of the Army position, unless so designated by other authorized documents.

The use of trade names or manufacturers' names in this report does not constitute indorsement of any commercial product.

REPORT DOCUMENTATION PAGE

Public reporting burden for this collection of information is estimated to average 1 hour per response, including the time for reviewing instructions, searching existing data sources, gathering and maintaining the data needed, and completing and reviewing the collection of information. Send comments regarding this burden estimate or any other aspect of this collection of information, including suggestions for reducing this burden, to Washington Headquarters Services, Directorate for Information Operations and Reports, 1215 Jefferson Davis Highway, Suite 1204, Arlington, VA 22202-4302, and to the Office of Management and Budget, Paperwork Reduction Project (0704-0188), Washington, DC 20503.

1. AGENCY USE ONLY (Leave blank)	2. REPORT DATE **September 1993**	3. REPORT TYPE AND DATES COVERED Final, Apr 92 - Dec 92	
4. TITLE AND SUBTITLE Aerodynamic Characteristics of a Helicopter Rotor Airfoil as Affected by Simulated Ballistic Damage			5. FUNDING NUMBERS 1L162618AH80
6. AUTHOR(S) J. Gordon Leishman			
7. PERFORMING ORGANIZATION NAME(S) AND ADDRESS(ES) University of Maryland Dept of Aerospace Engineering College Park, MD 20742			8. PERFORMING ORGANIZATION REPORT NUMBER
9. SPONSORING/MONITORING AGENCY NAME(S) AND ADDRESS(ES) U.S. Army Research Laboratory ATTN: AMSRL-OP-CI-B (Tech Lib) Aberdeen Proving Ground, MD 21005-5066			10. SPONSORING/MONITORING AGENCY REPORT NUMBER **ARL-CR-66**

11. SUPPLEMENTARY NOTES

The Project Officer for this report is Dr. Ki C. Kim, U.S. Army Research Laboratory, ATTN: AMSRL-SL-BA, Aberdeen Proving Ground, MD 21005-5068.

12a. DISTRIBUTION/AVAILABILITY STATEMENT Approved for public release; distribution is unlimited.	12b. DISTRIBUTION CODE

13. ABSTRACT (Maximum 200 words)

Tests were made in a two-dimensional insert at the University of Maryland's Glenn L. Martin subsonic wind tunnel to examine the effects of simulated ballistic damage on the aerodynamic characteristics of a UH-60A Black Hawk helicopter main rotor blade section. Tests were conducted on the undamaged blade section, and on the same section with simulated ballistic damage comprising a circular hole with a surrounding portion of the skin removed, exposing the internal honeycomb structure. The structural lift, drag and pitching moment were measured at small increments in angle of attack up through stall at Reynolds numbers of 10^6 and 2×10^6. In addition, tests were conducted over a full 360-degree range in angle of attack for a Reynolds number of 10^6. The measurements were complemented by mini-tuft flow visualization on the upper wing section, particularly near the hole. The effects of the simulated damage were found to cause large disturbances to the local flowfield near the hole. Separation was initiated at the upstream leading edge of the hole, followed by a growth in separation both in span and intensity with increasing angle of attack. The aerodynamic characteristics were found to be significantly degraded by the simulated ballistic damage, with a 20 percent reduction in lift curve slope, a loss of maximum lift capability of the order of 30 percent, and a significant decrease in the lift-to-drag ratio due to nearly a three-fold increase in sectional drag at low angles of attack.

14. SUBJECT TERMS rotor blades; aerodynamics; wind tunnel test; ballistic damage			15. NUMBER OF PAGES 56
			16. PRICE CODE
17. SECURITY CLASSIFICATION OF REPORT UNCLASSIFIED	18. SECURITY CLASSIFICATION OF THIS PAGE UNCLASSIFIED	19. SECURITY CLASSIFICATION OF ABSTRACT UNCLASSIFIED	20. LIMITATION OF ABSTRACT SAR

NSN 7540-01-280-5500

Standard Form 298 (Rev 2-89)
Prescribed by ANSI Std Z39-18
298-102

INTENTIONALLY LEFT BLANK.

Table of Contents

DTIC QUALITY INSPECTED 1

Accesion For		
NTIS CRA&I		☑
DTIC TAB		☐
Unannounced		☐
Justification		
By		
Distribution /		
Availability Codes		
Dist	Avail and / or Special	
A-1		

INTENTIONALLY LEFT BLANK.

List of Figures

List of Tables

INTENTIONALLY LEFT BLANK.

Acknowledgment

INTENTIONALLY LEFT BLANK.

Nomenclature

A	Wing area, ft^2
c	Airfoil chord, ft
C_D	Drag coefficient
C_{D_0}	Zero-lift drag coefficient
C_L	Lift coefficient
C_M	Pitching moment coefficient about the 1/4-chord
$dC_L/d\alpha$	Lift-curve-slope, $/deg$
f	Effective nondimensional location of separation point
q_∞	Free-stream dynamic pressure, lb/ft^2
Re	Reynolds number based on airfoil chord, $\rho V_\infty c/\mu_\infty$
V_∞	Free-stream velocity
W	Uncertainty in measurement quantity
x_{ac}	Nondimensional aerodynamic center location
x_{cp}	Nondimensional location of the center of pressure
α	Angle of attack, deg
α_0	Zero-lift angle of attack, deg
ρ_∞	Free-stream density, $slugs/ft^3$
μ_∞	Free-stream viscosity, $slugs/ft/s$

INTENTIONALLY LEFT BLANK.

I. Introduction

For military helicopters, rotor blade ballistic vulnerability is a major consideration. In a combat situation, these aircraft are exposed to a variety of armor piercing and high explosive incendiary projectiles from both ground and air-fire. Combat experience shows that rotor blades, particularly those of the main rotor, are often hit. While the rigorous application of advanced composite materials yields high levels of damage tolerance, ballistic damage to the blade(s) may still compromise the aerodynamic capabilities of the rotor system. Currently, with respect to vulnerability assessment, there is insufficient understanding on the effects of ballistic damage on the aerodynamic performance of helicopter rotor blades, or how damaged blades may compromise the helicopter performance, vibratory loads or aeroelastic stability of the rotor systems.

Even minor ballistic damage may present significant problems because of aerodynamic performance degradation of the rotor. At a minimum, a single area of damage on the blade may drastically increase the sectional drag and present an increased rotor torque (power) requirement. The loss of lift and change in section pitching moment, especially near the tip where the dynamic pressure is high, may present flight envelope restrictions such as a loss of payload capability, or reduced forward flight capability due to premature blade stall or high control forces. Other potential problems include the development of high structural vibrations generated by the damaged rotor systems that may be severe enough to compromise structural integrity or cause the crew to abort the mission or force land the aircraft.

Unsteady aerodynamic factors arising from ballistic damage also may be an issue. If the damage causes unsteady aerodynamic forces due to periodic flow separation, this may produce an in-plane or lead/lag excitation on the rotor blades. Since the lead/lag motion is the least damped degree-of-freedom on a rotor, this may produce aeroelastic problems. In fact, separation induced excitation is a very real possibility on rotors since the blade sections usually operate close to the angle of attack/Mach number stall boundary. Therefore, a quantitative understanding of the aerodynamic effects of ballistic damage is essential to assess accurately the level of vulnerability.

This report documents the first phase of a research program with the overall objective of quantifying the effects of simulated as well as actual ballistic damage on the aerodynamic characteristics of a helicopter main rotor blade section. The first phase of this project comprised the construction and validation of a test fixture, combined with experimental measurements of the aerodynamic characteristics of a short section of an actual UH-60A Black Hawk blade. This blade section was supplied by the U.S. Army Research Laboratory, Aberdeen Proving Ground, Maryland. A two foot span of the blade was subjected to prescribed damage in the form of a circular hole, and aerodynamically tested in a 2-D insert at the University of Maryland's Glenn L. Martin wind tunnel. The lift, drag and pitching moment characteristics as functions of angle of attack were compared to the undamaged (reference) blade section.

The results from this study have shown large effects of ballistic damage on the aerodynamic characteristics. The work has also enabled a much better quantitative understanding of the significance of ballistic damage on the aerodynamic characteristics of a typical rotor

blade section, and has provided a solid foundation for future research on the problem.

II. Description of the Experiment

1. Test Facility

The test were conducted in the Glenn L. Martin wind tunnel at the University of Maryland. This is a closed return tunnel with an 8-by-11 foot working section. Wind speeds of up to 300 feet per second (free-stream Mach number of 0.3) can be achieved in this tunnel, however, the present tests were conducted at more moderate wind speeds up to about 150 ft/s. This restriction was due to the high aerodynamic loads generated on the blade section and test fixture at higher wind speeds, which were beyond the capabilities of the force balance measurement system.

The test on the blade (wing) sections were made possible using a 2-D insert. This insert was specifically designed and built for these tests. The design and construction was carried out in-house at the Glenn L. Martin wind tunnel. The insert consisted of floor to ceiling false walls, and the test wing spanned these two walls, as shown in Fig. 1. A photograph of the insert (looking upstream) is shown in Fig. 2. The 2-D insert has the effect of reducing 3-D induced effects, in effect, making the wing appear to be of high aspect ratio, i.e., two-dimensional.

As detailed in Fig. 3, the insert walls comprised a NACA 0015 nose and trailing-edge section, with a flat center section. The center panels were manufactured from aluminum, and the leading and trailing edges from a foam core with a glass fiber skin. These leading edge and trailing edge panels were mounted to the main support by structural fasteners. The test wing was mounted between two recessed circular disks that were located flush with the flat center section of the insert sections. The circular disks were rotated by a wing pitch mechanism, which comprised a ring gear driven by a servo motor through a chain transmission. A displacement transducer was used to determine the angular position, and therefore, the wing geometric angle of attack.

The 2-D insert was able to accommodate test wings of up to 2.5 feet (30 inches) in chord. For the present test, the gap between the insert was set to 2 feet. However, provision has been made in the design to allow tests on wings with spans greater or smaller than 2 feet. The blade section was mounted to the pitch drive mechanism by mean of plugs that were fitted inside the titanium spar of the blade. Similar plugs can be made for other blade sections.

The entire wing support structure and pitch change mechanism was mounted on the 6-component wind-tunnel yoke balance system. All physical connections to the balance system were inside the insert walls by means of the structure detailed in Fig. 4. Using the balance

system, measurements could be made of the total wing lift, pitching moment and drag at any angle of attack between 0^0 and 360^0.

Because of the highly three-dimensional nature of the ballistic damage (usually a large hole with a ragged edge on one or both sides of the blade), obtaining the true 2-D aerodynamic properties of any one section of the blade is impractical. Therefore, the measured aerodynamic characteristics represent the effects of ballistic damage on a typical blade element of up to about half the test span (one foot). This is representative of the size of blade element discretization used in modern comprehensive rotor analyses [1-3].

2. Wing Section

The wing section used in this experiment was an actual section from the outer span of a UH-60A Black Hawk main rotor blade that had been removed from service. The wing section was refurbished to an aerodynamically smooth contour, and spray painted with a matte-black finish. Since the Black Hawk rotor blade has a pre-twisted angle (washout) of 18 degrees from root to tip, the test wing comprised about 1.5 degrees of twist along the span. This in-built twist was compensated for by defining a reference angle at mid-span that was equal to the average twist over the section.

The reference blade chord was 1.73 ft with a span of 2.0 ft, giving an undamaged reference area of 3.461 ft^2. The ballistic damage was simulated by means of a circular hole of 5 inches in diameter. This hole was drilled at the mid-span of the wing, and was located 0.75 ft downstream of the leading edge. Around the periphery of the hole, a one inch ring of the blade glass-fiber skin was removed to expose the paper honeycomb interior structure. Fig. 5 shows a sketch of the simulated damage configuration. With the clean hole, the effective load producing area of the wing was reduced by 0.1363 ft^2 giving a reference area with damage of 3.324 ft^2 or a wing area ratio of 0.96. If the removal of the skin was also considered, then the reduction in load producing area increased to 0.267 ft^2 giving a new reference area with damage of 3.193 ft^2 or a wing area ratio of 0.923. The reference area including skin removal was ultimately used to normalize the data for comparison with coefficients found using the undamaged reference area.

3. Data Acquisition

The entire data acquisition process was controlled by a HP-A900 computer. A custom data acquisition routine was written using Hewlett-Packard's VEE (Virtual Engineering Environment) to control the angle of attack schedule, and acquire measurements of the loads. The lift, drag and pitching moment were sampled several times at each test condition, and the final measurement was an average acquired to within a prescribed tolerance and statistical accuracy. The measurements were plotted on a graphics monitor in real-time using IDL graphics routines.

The dynamic pressure in the working section was measured indirectly in terms of a pressure drop between the static pressure measured in the settling chamber, and the average static pressure measured at a ring of orifices at the forward upstream end of the working section. The relationship between the pressure drop and the actual dynamic pressure in the working section was obtained by means of a calibration. For this, a NASA calibrated pitot static probe was located in the tunnel working section at the wing location, but without the wing installed. The measured dynamic pressure at this position was correlated with the pressure drop between the settling chamber and the forward wall pressure.

During the tests, the dynamic pressure was maintained as closely as possible to the required value by careful adjustment of the fan rpm. With increasing wing angle of attack, the increased solid and wake blockage produced by the wing requires a higher fan power and rpm to maintain a constant dynamic pressure in the working section. During some tests at high angles of attack, periodic separation and reattachment and/or vortex shedding made it difficult to maintain a constant dynamic pressure. Under these conditions, the measurements of the aerodynamic characteristics to a specified precision are difficult or impossible, and the final values, therefore, have a higher overall uncertainty.

4. Test Conditions

A summary of the test conditions are given in Table 1. Experiments on undamaged and damaged blade sections were conducted at two Reynolds numbers of 10^6 and 2×10^6. Since the airfoil was nonsymmetric, it was necessary to examine both the negative and positive angle of attack ranges up through stall. Tests were normally conducted over an angle of attack range from -5 degrees to 25 degrees, and from 5 degrees to -25 degrees in steps of one degree. This provided results over the typical working range of a helicopter rotor blade section. Smaller angle of attack increments were taken near the maximum lift conditions, in order to accurately define the stall characteristic.

It should be noted that different stall characteristics were obtained at different Reynolds numbers as well as at negative and positive angles of attack. In addition, both increasing and decreasing angle of attack sweeps were made, since static hysteresis effects can occur, particularly at low Mach numbers and low Reynolds numbers. In the present case, static hysteresis effects were found to be minor. For a Reynolds number of 10^6, tests were also conducted over a full 360 degrees of angle of attack. The angle of attack increment in this range was normally five degrees. It was not practical to conduct full 360 degree angle of attack sweeps at the higher Reynolds number due to the high loads imposed on the support and balance system.

Deadweight tares were obtained from balance measurements with the wing installed but with the wind off. Tares were obtained over the required range of angles of attack, and curve fitted to obtain the appropriate corrections at intermediate angles of attack. These tares were automatically subtracted from the measurements.

4

5. Experimental Accuracy

The VEE balance data acquisition program requires that the desired precision of each force or moment component be specified in dimensional form. Realistic limits for the precision of components was ± 0.1 lb_f on force components and ± 0.5 $in\text{-}lb$ on moment components. The precision achievable in practice depends on the unsteadiness of the loads. In this experiment, the balance loads were obtained to a target precision of the mean based on an equation of the form

$$P = \frac{k\sigma}{\sqrt{n}} \tag{1}$$

where P is the target precision, σ is the standard deviation, n is the number of samples acquired, and k is a factor which is a function of the level of confidence and the number of samples. At angles of attack where stall and extreme buffeting occurs, the precision was occasionally relaxed in order to keep total data acquisition time within reasonable limits.

The results were converted into sectional or coefficient values by normalizing by dynamic pressure and a reference wing area. For the undamaged wing, the force coefficients were obtained from

$$C_L = \frac{L}{q_\infty A} \tag{2}$$

$$C_D = \frac{D}{q_\infty A} \tag{3}$$

and the moment coefficient about the 1/4-chord from

$$C_M = \frac{M}{q_\infty A c} \tag{4}$$

where A is the undamaged wing reference area, and c is the blade chord. For the damaged wing, the force and moment coefficients were obtained in two forms. The first was obtained by normalizing using the undamaged wing area, as above. This served to show the combined effect of simulated damage due to both a reduction in lifting or load producing area as well as the alteration in the 3-D flow separation characteristics of the wing section. The second form of force and moment coefficients were obtained by normalizing with respect to the damaged wing area. This helps to isolate the other flow effects from the reduction in aerodynamic load bearing area in the measurements.

The error in the measurements of the aerodynamic coefficients is a function of the uncertainty of the measurements. The uncertainty, W_{C_L}, in the lift coefficient, C_L, is given by

$$W_{C_L} = [(\frac{\partial C_L}{\partial L} W_L)^2 + (\frac{\partial C_L}{\partial q_\infty} W_{q_\infty})^2 + (\frac{\partial C_L}{\partial A} W_A)^2]^{1/2} \qquad (5)$$

where W_L, W_{q_∞} and W_A are the errors in the measurement of the lift force, the free-stream dynamic pressure, and the wing area, respectively. These estimated errors are summarized in Table 4.

The preceding equation (Eq. 5) may be simplified to obtain the relative error in C_L, giving

$$\frac{W_{C_L}}{C_L} = [(\frac{W_L}{L})^2 + (\frac{W_{q_\infty}}{q_\infty})^2 + (\frac{W_A}{A})^2]^{1/2} \qquad (6)$$

Similar equations can be derived to obtain the error in the measurements of C_M and C_D. In general, the errors in the force and moment coefficient were found to be less than 0.1% under all conditions, except when periodic flow separation occurred on the wing. This latter situation is discussed later in this report.

6. Flow Visualization

A limited amount of flow visualization was conducted using mini-tufts. The tufts were placed on the upper surface of the wing, and on the walls of the 2-D insert. The tufts provided a good qualitative understanding of the nature of the flow environment at the wing/wall juncture, as well as due to the presence of the simulated ballistic damage. Still photographs and video were used to document the development of flow separation on the wing up through stall. The video was particularly useful near stall onset, since here the flow was often unsteady due intermittent flow separation and reattachment.

7. Wall Pressure Signatures

In addition to the force and moment measurements, pressure measurements were also made on the walls of the 2-D insert. This information has been used to help evaluate the flow quality and longitudinal pressure gradient in the test section, and will ultimately be used to assist in the preparation of corrections to the measured data. This was not within the scope of the present work, and has been left as a longer term goal. Therefore, all the present measurements are presented without the application of correction factors.

III. Results and Discussion

1. Aerodynamics of Undamaged Airfoil

Figures 6 through 8 show the aerodynamic characteristics of the baseline airfoil, as measured at Reynolds numbers of 10^6 and 2×10^6. The results are typical for a cambered airfoil at low Mach number. Note that in the attached flow regime, the lift and pitching moment vary linearly with angle of attack, and the drag exhibits a parabolic variation.

The results measured in the attached flow region can be used to extract key aerodynamic characteristics, such as lift-curve-slope, zero lift angle, and the location of the aerodynamic center. The lift-curve-slope and zero lift angle (intercept on α-axis) were obtained from a least square fit [4] to the measured data in the attached flow regime using the equation

$$C_L = \frac{dC_L}{d\alpha}(\alpha - \alpha_0) = C_{L_a}(\alpha - \alpha_0) \tag{7}$$

Similarly, the zero lift drag coefficient was obtained in a least squares sense using the equation

$$C_D = C_{D_0} + C_{D_1}(\alpha - \alpha_0) + C_{D_2}(\alpha - \alpha_0)^2 \tag{8}$$

The nondimensional position of the aerodynamic center was obtained from the lift curve slope and the moment curve slope using

$$x_{ac} = \frac{1}{4} - \frac{dC_M}{dCL} = \frac{1}{4} - (\frac{dC_M}{d\alpha})(\frac{d\alpha}{dC_L}) \tag{9}$$

A summary of the measured aerodynamic parameters for the undamaged airfoil in the attached flow regime are given in Table 2.

The behavior of the airfoil at angles of attack near maximum lift are of significant interest. Since the airfoil was nonsymmetric, both the stall at positive and negative angles of attack were examined in this experiment. For the positive angle of attack regime at the lower Reynolds number, the airfoil exhibits a trailing-edge stall mechanism. Here, flow separation begins at the trailing edge and moves toward the leading edge. This mechanism can be easily inferred from the lift characteristics, where the lift-curve-slope shows a progressively greater nonlinear behavior near maximum lift, and is consistent with the effects produced by the gradual forward movement of trailing-edge separation. The stall mechanism is further confirmed by the pitching moment behavior, where the trend toward a decreasing nose down

moment near maximum lift is also characteristics of airfoils that exhibit stall by the trailing-edge separation mechanism.

At the higher Reynolds number of 2×10^6, Fig. 6 shows that the stall onset became more abrupt; however, the stall mechanism was still upstream or forward movement of trailing-edge separation. Increasing stall abruptness with increasing Reynolds number is characteristic of cambered airfoils in the low Mach number regime. Note that at the higher Reynolds number, slightly higher values of maximum lift are obtained, which is again a well known characteristic of airfoils with increasing Reynolds number at a nominally constant Mach number.

At negative angles of attack at the same Reynolds number of 10^6, the stall mechanism also appears to be by the gradual forward movement of trailing edge separation. However, recall that this time the flow separation develops on the lower surface of the airfoil. Since the lower airfoil contour is not designed to control the high adverse pressure gradients that occur at large negative angles of attack, rapid boundary layer thickening and separation occurs on the lower surface, even at moderately low negative angles of attack. This results in a progressive rounding of the lift-curve-slope and a fairly low value of maximum negative lift. At the higher Reynolds number of 2×10^6, it will be seen that the negative stall characteristic is subsequently more abrupt, with a slight increase in maximum negative lift compared to a Reynolds number of 10^6.

Tests were also conducted to determine the existence of any static hysteresis effects in the measurements. Because of the differences in the physical processes of flow separation versus flow reattachment, it is known that under some circumstances different values of the airloads can be obtained depending on the actual test technique. For example, at high angles of attack different results can be obtained for a series of angles of attack depending on whether the angle of attack is continuously incremented or decremented over this range. Similarly, different results can be obtained if the angle of attack is set first and the wind speed increased to the required conditions, versus setting the wind speed and then incrementing the angle of attack. This phenomenon is usually referred to as "static hysteresis".

Measurements made for increasing and decreasing sweeps in angle of attack are shown in Fig. 9 for a constant Reynolds number of 2×10^6. It can be seen that static hysteresis effects are small, and are mostly confined to small range in angle of attack in the post stall regime. Overall, the effects were considered to be sufficiently inconsequential that all further tests were conducted with a positive angle of attack increment in the positive angle of attack regime, and with a negative increment in the negative angle of attack regime.

2. Aerodynamics of Damaged Airfoil

The effects of ballistic damage were simulated by means of a circular hole with a portion of the surrounding skin removed, as discussed previously (see section 2.2). A comparison of the measured aerodynamic characteristics for the undamaged and damaged airfoils is shown Figs. 10 through 12 for a Reynolds number of 10^6 and in Figs. 13 through 15 for a Reynolds number of 2×10^6. All force and moment coefficients are initially normalized with respect

8

to the undamaged (reference) wing area.

Several results were immediately apparent. Considering the lift, as shown in Figs. 10 and 13, it is clear that the lift-curve-slope and maximum lift coefficient are significantly less for the damaged airfoil. The flow visualization results showed that flow separation occurred at the upstream edge of the hole, therefore the reduction in both the lift-curve-slope and maximum lift are consistent with this observation.

The prediction of maximum lift on an airfoil is difficult under any circumstances; however, it is possible to estimate the reduction in lift curve slope of an airfoil with a fixed separation point by means of Kirchhoff theory [5]. If it is assumed that the airfoil is sufficiently thin that it can be approximated by a flat plate, then Kirchhoff theory gives a relationship between the lift coefficient, the angle of attack, and the trailing edge separation point as

$$C_L = \frac{dC_L}{d\alpha}(\frac{1+\sqrt{f}}{2})^2(\alpha - \alpha_0) \tag{10}$$

where f is the non-dimensional location of the effective separation point, and $dC_L/d\alpha$ is the lift-curve-slope of the undamaged airfoil section. For the conditions here, it can be assumed that the mean effective flow separation point is fixed at the mid-point of the hole (55% of chord at mid-span). The reduction in lift-curve-slope can be approximately estimated by substituting a fixed separation point of $f = 0.55$ in Eq. 10. This gives the effective lift-curve-slope of the damaged airfoil as

$$(\frac{dC_L}{d\alpha})_{damaged} = (\frac{1+\sqrt{0.55}}{2})^2(\frac{dC_L}{d\alpha})_{undamaged} = 0.76(\frac{dC_L}{d\alpha})_{undamaged} \tag{11}$$

This result compares very favorably with the measured reduction in lift-curve-slope of about 80% obtained at both Reynolds numbers.

For other locations of damage on the airfoil, it is plausible that the Kirchhoff theory can be used as a means of predicting the reduction in lift-curve-slope due to the development of separation. For example, Fig. 16 shows the ratio of the reduction in lift-curve-slope as a function of effective separation point. Clearly, for separation initiated at the leading-edge of the airfoil, the effects on the lift-curve-slope are more significant. Note however, that the validity of the Kirchhoff theory to the ballistic damage problem, in general, must still be validated. This will require experimental measurements as a function of hole size and chordwise position.

Note also from Figs. 10 and 13 that the overall stall characteristics is affected by the effects of damage, with a more gradual rounding of the lift curve near maximum lift. The premature onset of trailing-edge separation, due to the existence of the hole, limits the building-up in circulation, and by that reduces the maximum attainable value of lift by about 30%. However, note that the static stall angle, that is the angle of attack corresponding to the maximum lift coefficient, is relatively unaffected by the damage.

The corresponding pitching moment behavior is shown in Figs. 11 and 14 for the two Reynolds numbers. As shown previously, the effects of damage on the aerodynamic center location (i.e., the slope of the moment curve in the attached flow regime) is somewhat minor, but a slight forward movement of the aerodynamic center occurs relative to the undamaged case. Since the effects of damage promote premature trailing-edge separation, this shows as a more pronounced nose-up moment trend near the stall angle. This effect is apparent at both Reynolds numbers.

It is interesting that the magnitude of the post stall pitching moment is less for the damaged airfoil. Since the presence of the hole reduces the lifting area of the wing, the center of pressure stabilizes at a chordwise position closer to the quarter-chord moment axis. Again, this is the case at both Reynolds numbers.

The actual variation in the center of pressure with angle of attack is shown in Fig. 17 for $Re = 10^6$ and in Fig. 18 for $Re = 2 \times 10^6$, again with and without the simulated ballistic damage. The non-dimensional position of the center of pressure, x_{cp}, was computed from the pitching moment coefficient about the 1/4-chord, C_M, and the normal force coefficient, C_N using

$$x_{cp} = \frac{1}{4} - \frac{C_M}{C_N} \tag{12}$$

where

$$C_N = C_L \cos \alpha + C_D \sin \alpha \tag{13}$$

Note that the center of pressure measurements for both Reynolds numbers are very similar. In the positive low angle of attack regime, the center of pressure is close to the 1/4-chord. In fact, the center of pressure asymptotes to the location of the aerodynamic center prior to the development of flow separation and stall. After separation occurs at about 13 degrees angle of attack, the center of pressure moves quickly aft and asymptotes to about 40-50% chord. Note that the actual position of the center of pressure is only very weakly affected by the simulated ballistic damage, but lies slightly further forward than for the undamaged case.

Of the three aerodynamic load components, the effects of damage on the drag coefficient are perhaps the most dramatic. Figs. 12 and 15 show the variation in drag coefficient for the undamaged and damaged airfoils. It will be apparent that in the low angle of attack regime, the drag of the damaged airfoil is at least twice that of the undamaged airfoil, and for the higher Reynolds number the increase is almost three-fold. Again, this is because of the premature onset of trailing-edge flow separation, which limits the build-up of circulation and by that reduces the leading-edge suction and increases the pressure drag at a given angle of attack. In addition, there are rotational losses in the separated wake, which contributes further to the overall increase in drag. Figs. 19 and 20 show the variation in lift-to-drag ratio for the damaged and undamaged airfoils.

Table 3 gives a summary comparison of the measured aerodynamic characteristics of the damaged and undamaged wing section in the low angle of attack regime.

An alternative method of comparing the measured aerodynamic characteristics, is to normalize the results for the damaged wing by the damaged wing reference area. This helps to isolate the effects of a reduction in wing area to the aerodynamic problem. By including the effects of both the hole and the skin removal surrounding the hole, the ratio of the damaged wing area to the undamaged area is approximately 0.92. The effects of this alternative comparison is shown in Figs. 21 through 23 for a Reynolds number of 10^6. Clearly, it is not possible to reconcile the measurements by means of a simple correction on the basis of area removal due to the ballistic damage.

3. Aerodynamic Characteristics in Reverse Flow

In high speed forward flight, the inboard sections of the retreating blade will experience reverse flow. This occurs because the forward flight velocity is greater than the local velocity at the blade element due to rotation about the shaft. Although the dynamic pressure in the reverse flow region is relatively small, the center of pressure moves to the vicinity of the 3/4-chord location, and even with a low dynamic pressure this may produce a significant blade pitching moment.

The measured aerodynamic characteristics in the reverse flow region are shown in Figs. 24 through 26. Here, the sharp trailing-edge of the blade is pointing into the relative wind, and the rounded nose of the airfoil now becomes the trailing-edge. It will be seen that the aerodynamic characteristics in the low angle of attack regime still remain fairly linear with angle of attack, but the aerodynamic center is now close to the 3/4-chord, and consequently this produces much higher aerodynamic pitching moments about the 1/4-chord measurement axis. The onset of significant separation and stall occurs at a relatively low angle of attack, with a correspondingly low value of maximum lift and both negative and positive angles of attack.

Fig. 26 shows that the relaxation of the Kutta condition (accompanied by the separation at the now "blunt" trailing edge) produces a rather higher drag coefficient in reverse flow. Both the zero-lift drag coefficient and the increase in drag with increasing angle of attack are much larger than when the airfoil is operating in the normal flow regime. Note that the effects of the simulated ballistic damage are somewhat minor when the airfoil is operating in the reverse flow regime since the sharp leading-edge already degrades the aerodynamic performance of the airfoil.

4. Aerodynamic Characteristics in the High Angle of Attack Regime

Test over a full 360 degrees of angle of attack were conducted at a Reynolds number of 10^6. Tests at higher Reynolds numbers were not conducted due to the large unsteady

loads and severe buffeting associated with the flow about the airfoil at large angles of attack. For angles of attack greater than 30 degrees, there is massive flow separation over the top surface of the wing. Under these conditions, the flow is relatively unsteady and the loads vary in a more random fashion. However, under certain conditions, it is possible for the flow to "lock-in" and produce periodic vortex shedding. This induces large periodic loads on the wing, support structure, and balance system.

A summary of the measured aerodynamic characteristics of the undamaged and damaged wing are shown in Figs. 27 through 29. Note from Fig. 27 that in the post stall regime, the lift increases again, after that reducing progressively in magnitude up to 90 degrees angle of attack. The effects of damage obviously have only a small influence on the lift in the post-stall regime. On the other hand, both the pitching moment, as given in Fig. 28, and the drag, as given by Fig. 29, show a somewhat large effect of ballistic damage. The effects of the damage causes the center of pressure remain a little less aft than for the undamaged case, so the pitching moment coefficients are a little lower. Due to the reduced cross-sectional area of the damaged wing, the peak drag coefficient of the damaged wing shown in Fig. 29 is about 20% lower than for the undamaged wing. Note that for angles of attack between 100 degrees and 130 degrees, the measurements show somewhat more scatter. This is because of the occurrence of periodic vortex shedding from the wing over this angle of attack range.

5. Flow Visualization

Limited flow visualization was performed using mini-tufts attached to the top wing surface and to the side-walls of the 2-D insert. The tufts permitted a qualitative understanding of the flow environment at the wing/side-wall juncture, as well as a good understanding of the effects of the damage on the flow developments on the wing itself.

The mini-tufts are of low mass and stiffness, and respond quickly to changes in flow state. In regions where the flow is attached, the tufts align themselves flat with the surface and parallel to the local flow direction. In regions of flow separation, the tufts generally show a more random behavior, and are often raised from the wing surface. In regions of massive flow separation, the tufts are often aligned such that they are pointing in an upstream direction due to the flow recirculation in the separated flow region.

The flow visualization experiments were performed at various angles of attack up through stall. The results were recorded on conventional black and white film, as well as video tape. The video was useful for recording the highly dynamic behavior of the tufts near stall or in the separated flow near the damaged region of the wing. On the still photographs, a blurring of the tuft image indicates the unsteady flow.

A few sample flow visualization results are shown in Fig. 30. The presence of the simulated ballistic damage will be seen to cause flow separation at the upstream edge of the hole, even at low angles of attack. This is reflected in the drag measurements shown previously in Figs. 12 and 15, by which the increased separation produces an energy loss that shows up as an increase in drag.

For increasing angle of attack, the region of flow separation will be seen to expand and extend over a larger part of the wing trailing edge. Note also that the tufts at the outer span show that the flow over the outer (attached flow) part of the wing is affected, with the flow being directed toward the insert walls. These results confirm that the effects of ballistic damage are not necessarily confined to regions in the immediate region of the damage. Rather, the aerodynamic effects of ballistic damage may be felt over a span two or three times that of the dimensions of the damage.

IV. Summary and Conclusions

Tests were made in a two-dimensional insert at the University of Maryland's Glenn L. Martin subsonic wind tunnel to examine the effects of simulated ballistic damage on the aerodynamic characteristics of a UH-60A helicopter main rotor blade section. Tests were conducted on the undamaged blade section, and on the same section with simulated ballistic damaged comprising a circular hole with a surrounding portion of the skin removed exposing the internal honeycomb structure. The sectional lift, drag and pitching moment were measured at small increments in angle of attack up through stall at Reynolds numbers of 10^6 and 2×10^6. In addition, tests were conducted over a full 360 degree range in angle of attack for a Reynolds number of 10^6. The measurements were complemented by mini-tuft flow visualization on the upper wing section, particularly near the hole.

The following conclusions have been drawn from this study:

1. The effects of the simulated damage were found to cause large effects on the local flowfield near the hole. Separation was initiated at the upstream leading edge of the hole, followed by a growth in separation both in span and intensity with increasing angle of attack.

2. The overall aerodynamic characteristics were found to be significantly degraded by the simulated ballistic damage, with a loss of lifting performance and an increase in drag.

3. Approximately a 20% reduction in lift-curve-slope was obtained with the damage prescribed in this experiment. However, the reduction in lift-curve-slope due to damage is expected to be a strong function of the actual chordwise location of the damaged region on the blade.

4. If it is assumed that the location of the damaged region on the wing fixes the position of flow separation, Kirchhoff theory was shown to be an effective means of approximately predicting the corresponding reduction in lift-curve-slope. However, the generality of this model must be further explored.

5. With ballistic damage, there was a loss of maximum lift capability of the order of 30%. Again, the relative loss in maximum lift is expected to be a function of the actual chordwise location and extent of the ballistic damage.

6. The aerodynamic pitching moment was found to be only moderately affected by the simulated ballistic damage. The effect of the hole was to cause a small forward movement in the aerodynamic center location, and in the post-stall regime the center of pressure was found to stabilize slightly further forward than for the undamaged section.

7. Of all the aerodynamic characteristics, the simulated ballistic damage were found to have the largest effects on the drag. Depending on the Reynolds number, the drag coefficient of the damaged wing was found to be between two and three times that of the undamaged wing.
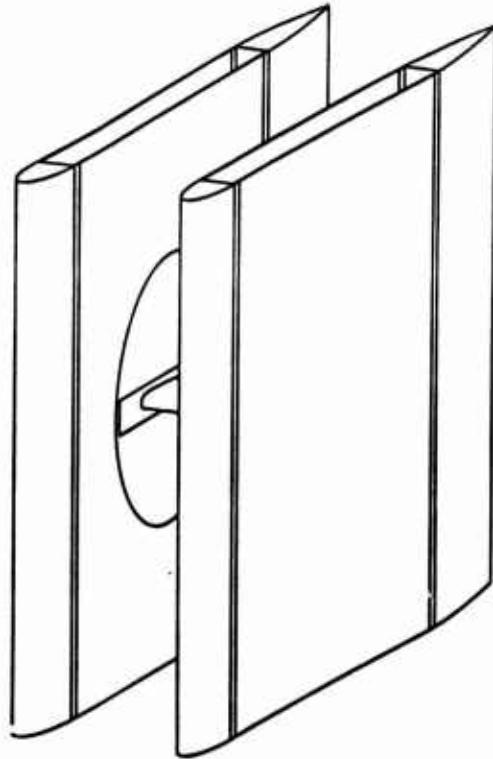
Two Dimensional Test Section Insert
Isometric view

Figure 1:   Isometric Sketch Showing Composition of 2-D Insert.
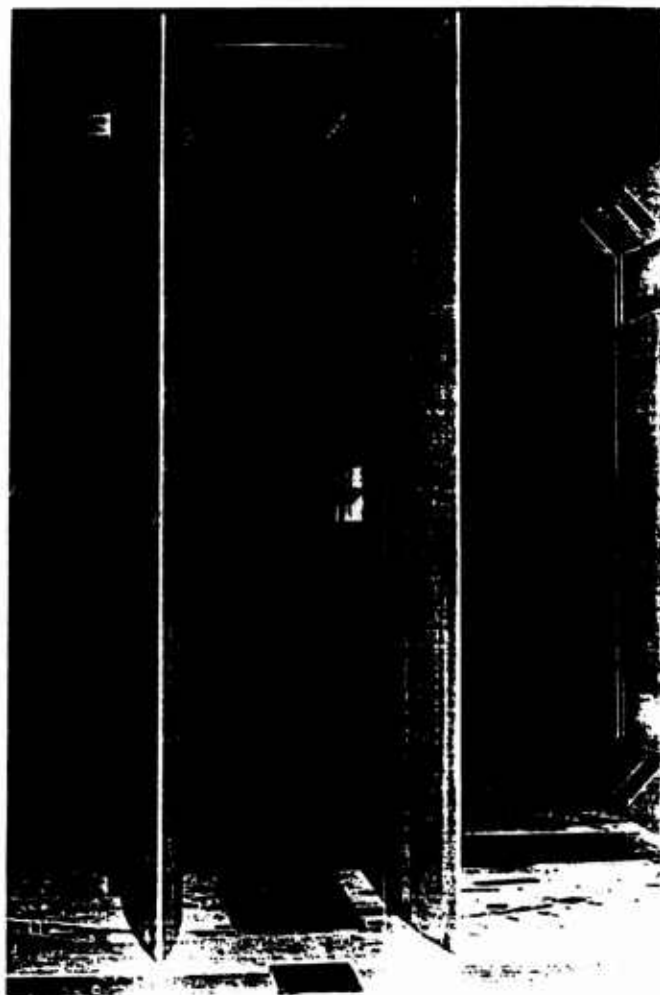
Figure 2:   Photograph of 2-D Insert, Looking Upstream.
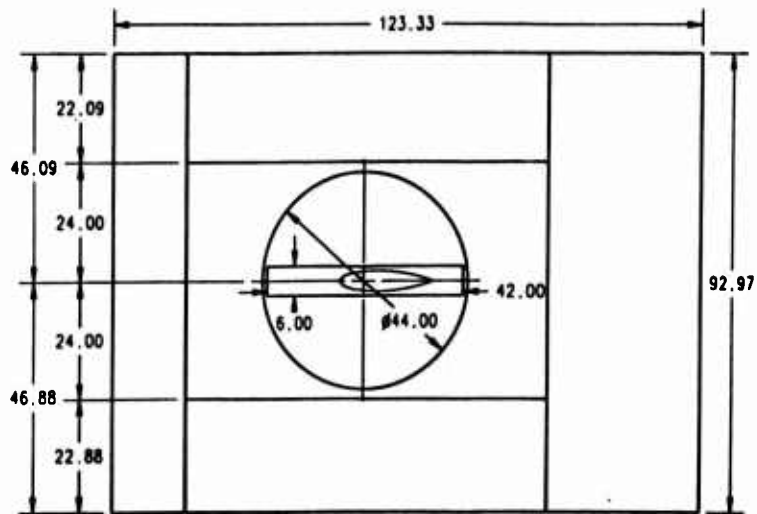
Side View
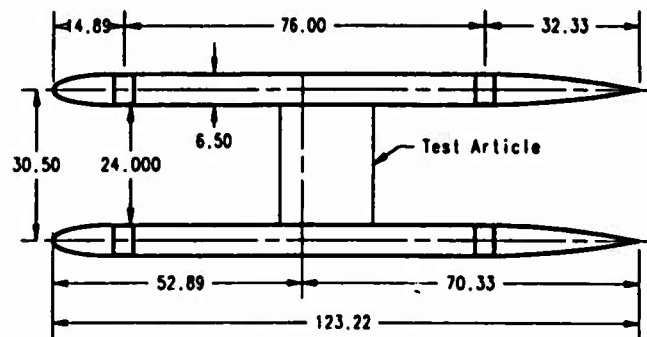
Two Dimensional Test Section Insert
Top View

Figure 3: 2-D Insert - Side View and Top View.
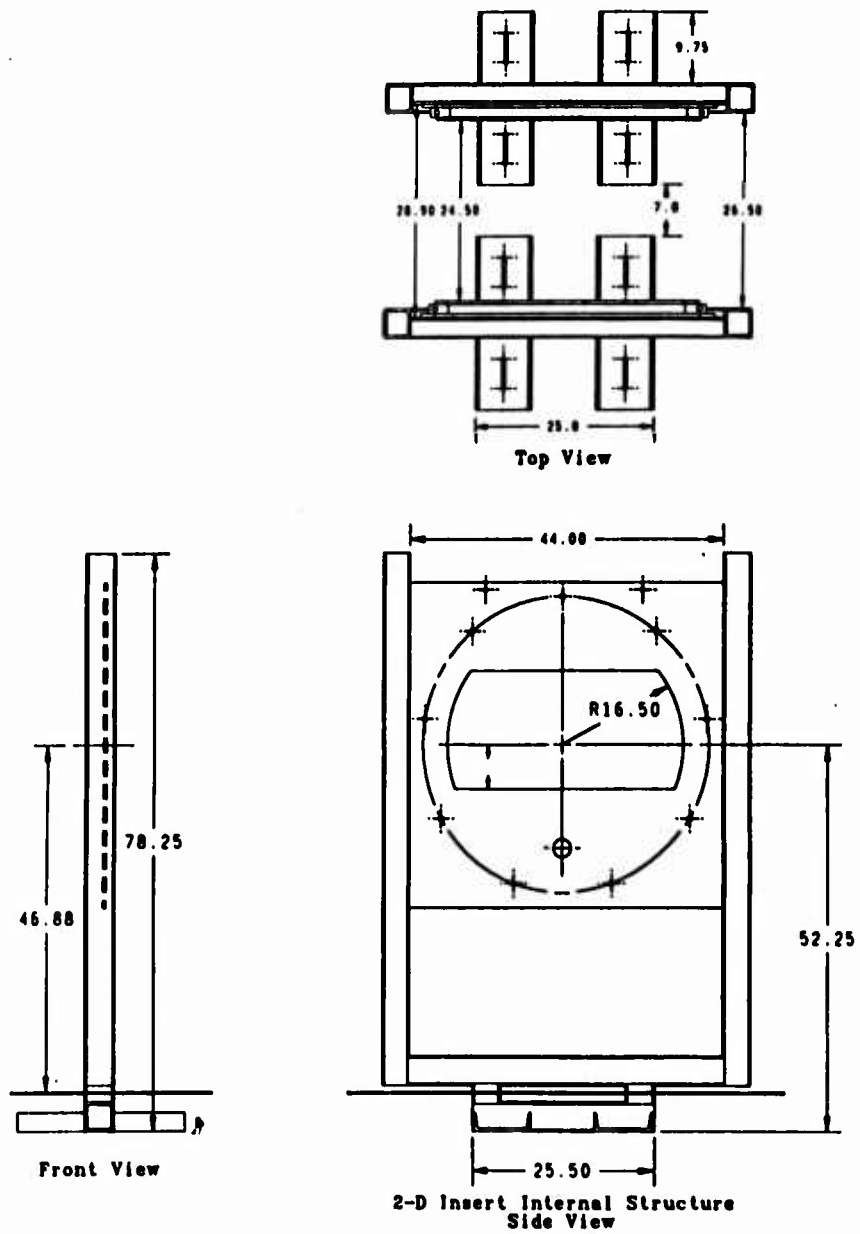
Figure 4:   2-D Insert Internal Structure - Side View, Front View and Top View.
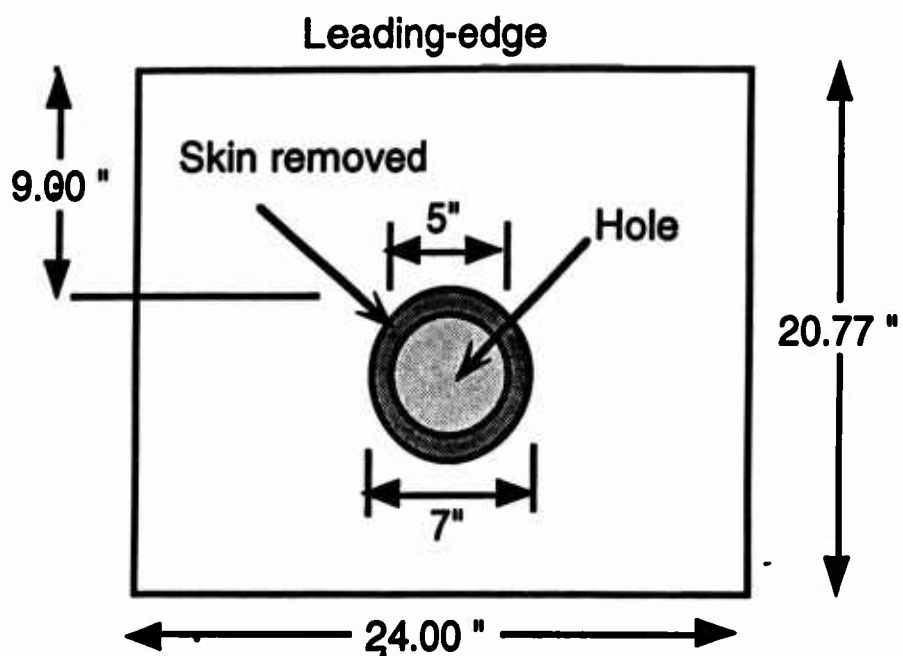
Figure 5: Sketch Showing Geometry of Simulated Ballistic Damage on the Test Wing.
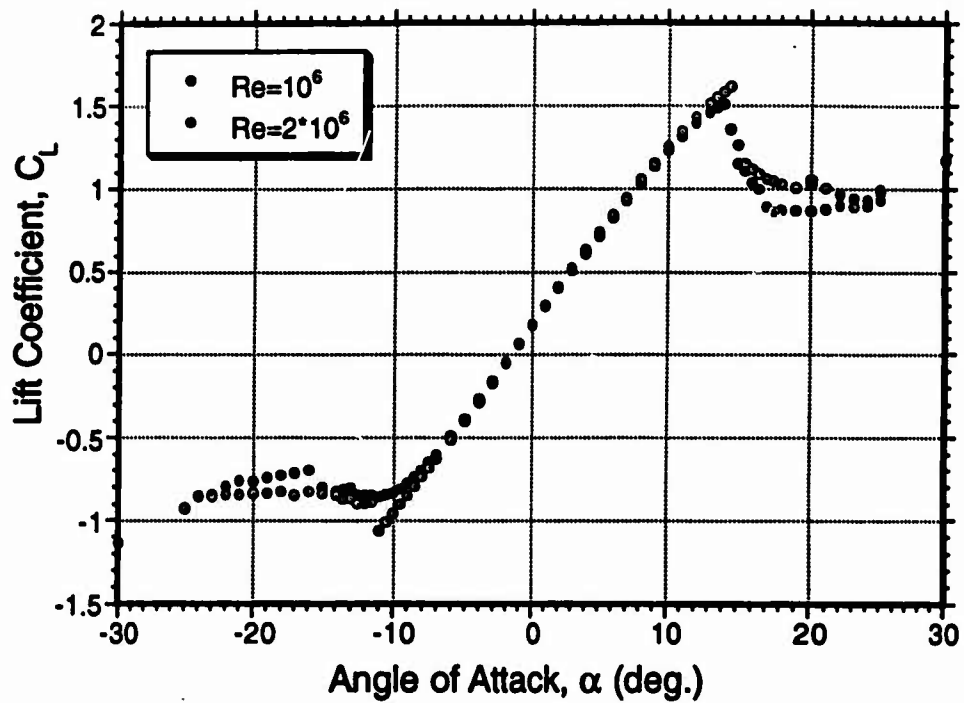
Figure 6: Lift Coefficient vs. Angle of Attack for Undamaged Airfoil.
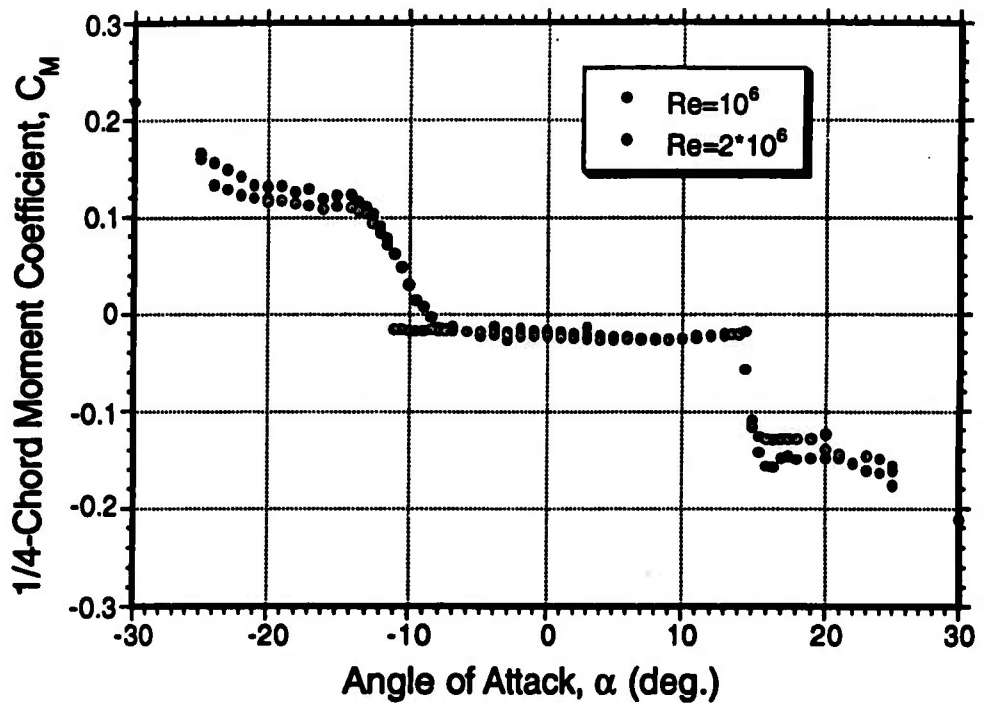
Figure 7: 1/4-Chord Pitching Moment Coefficient vs. Angle of Attack for Undamaged Airfoil.
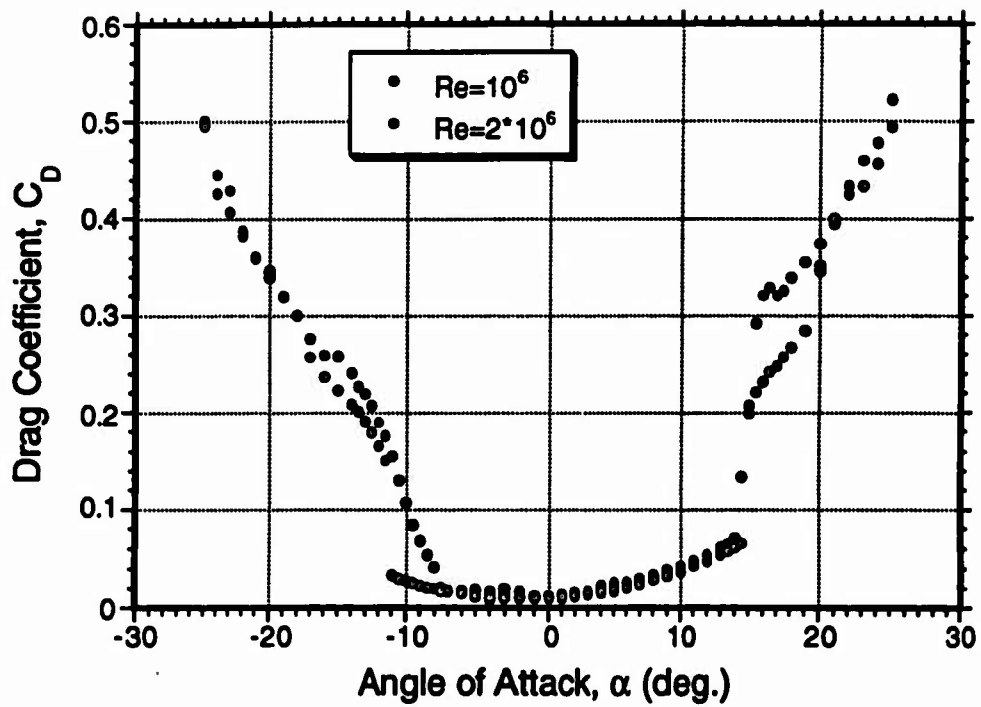
Figure 8: Drag Coefficient vs. Angle of Attack for Undamaged Airfoil.
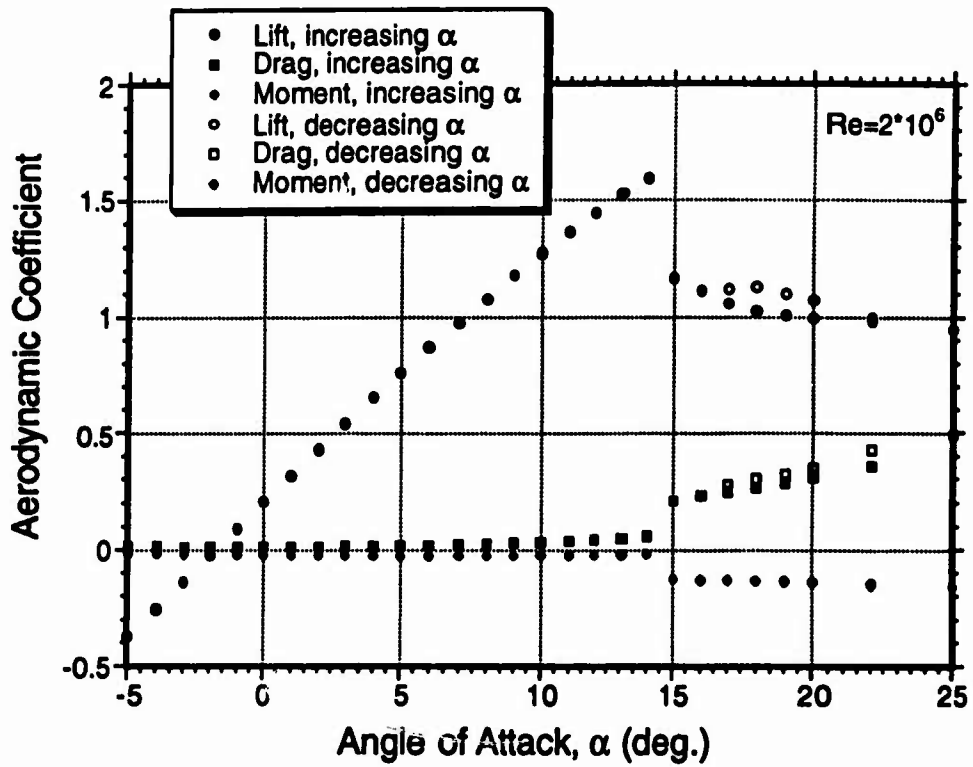
Figure 9: Static Hysteresis in Aerodynamic Coefficients for Undamaged Airfoil.
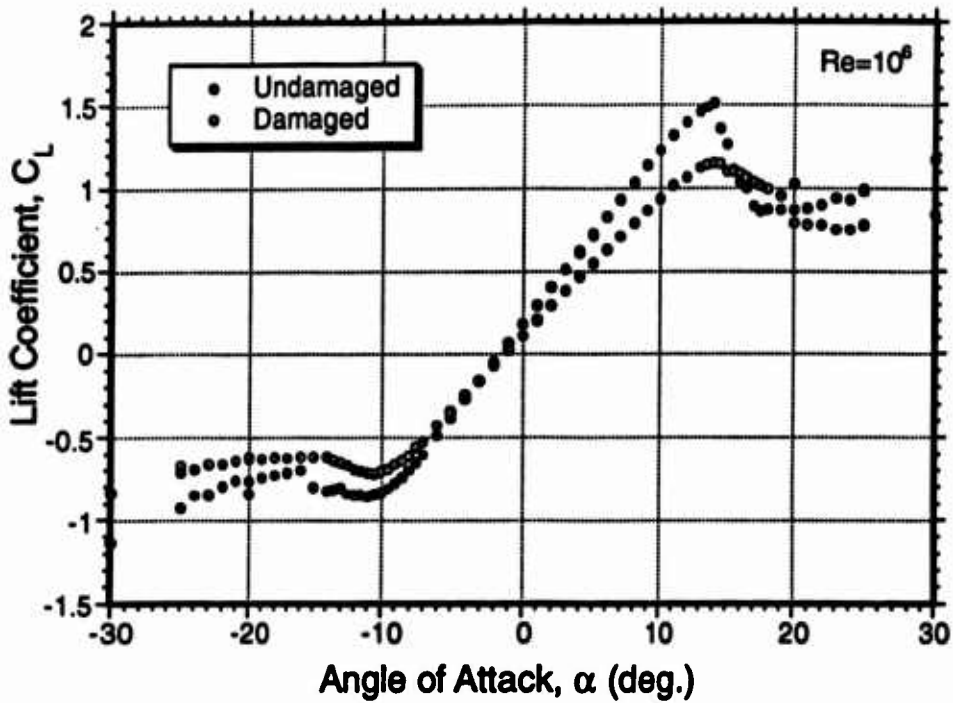
Figure 10:   Lift Coefficient vs. Angle of Attack for Undamaged and Damaged Airfoils, $Re = 1 \times 10^6$.
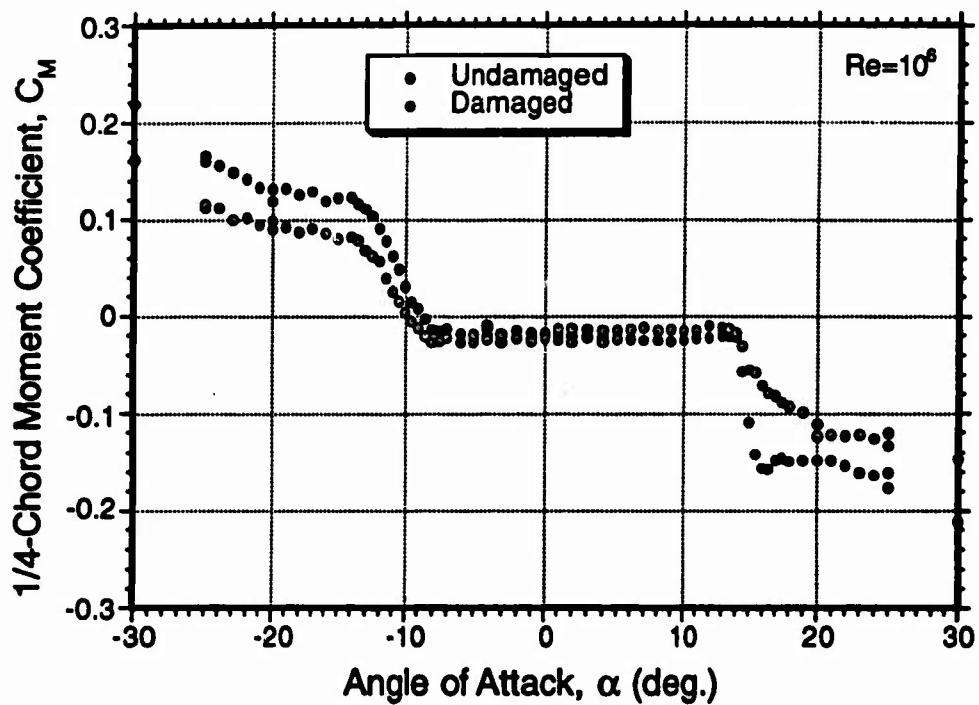
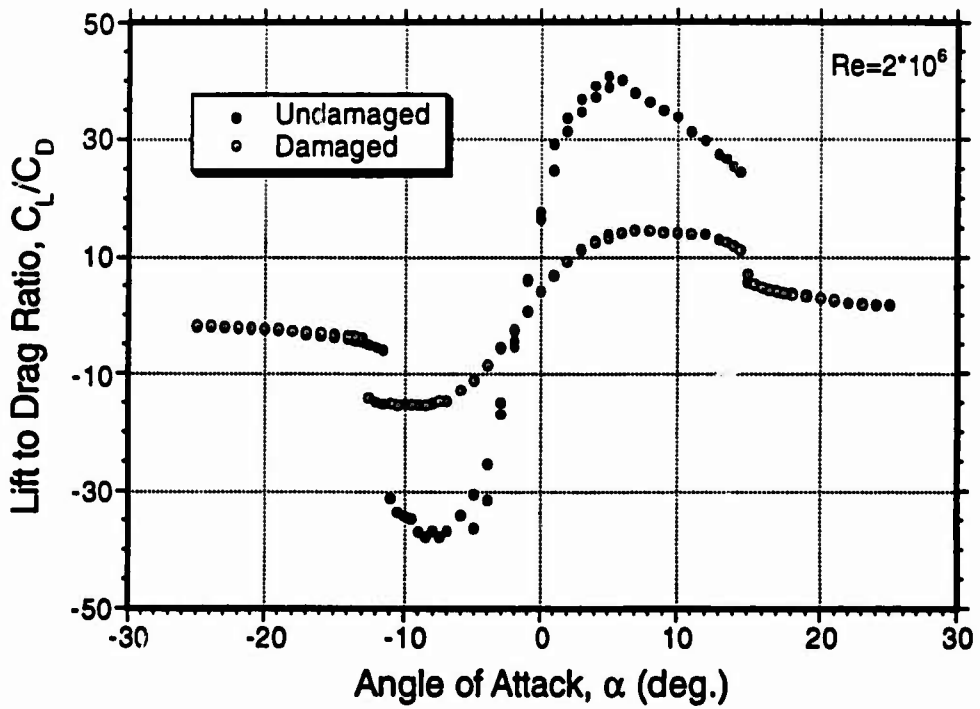Figure 11: Moment Coefficient vs. Angle of Attack for Undamaged and Damaged Airfoils, $Re = 1 \times 10^6$.
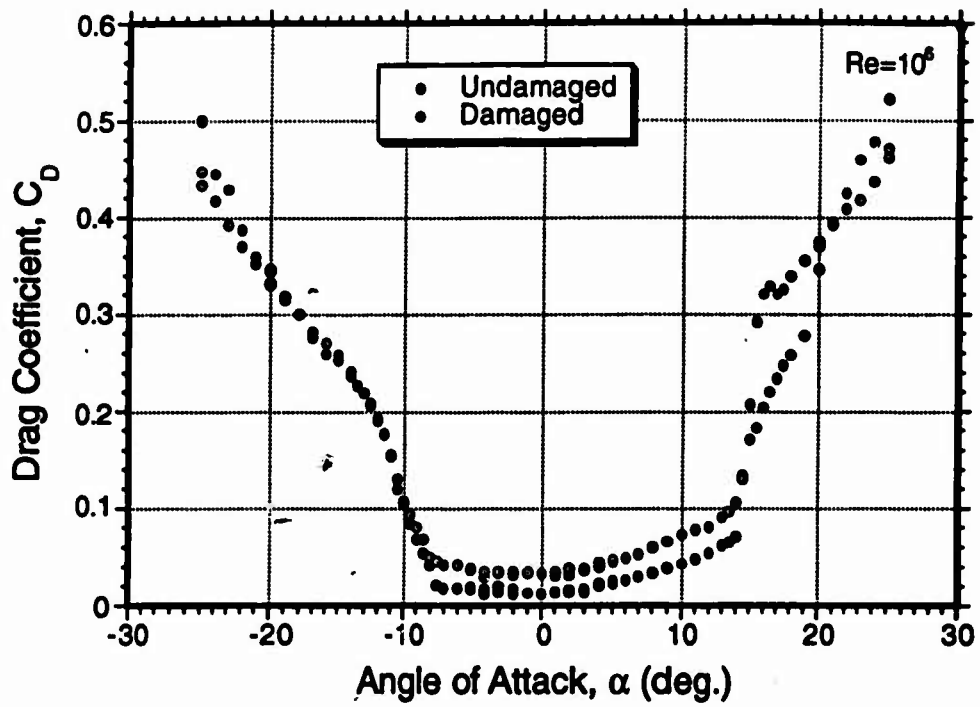
Figure 12: Drag Coefficient vs. Angle of Attack for Undamaged and Damaged Airfoils, $Re = 1 \times 10^6$.
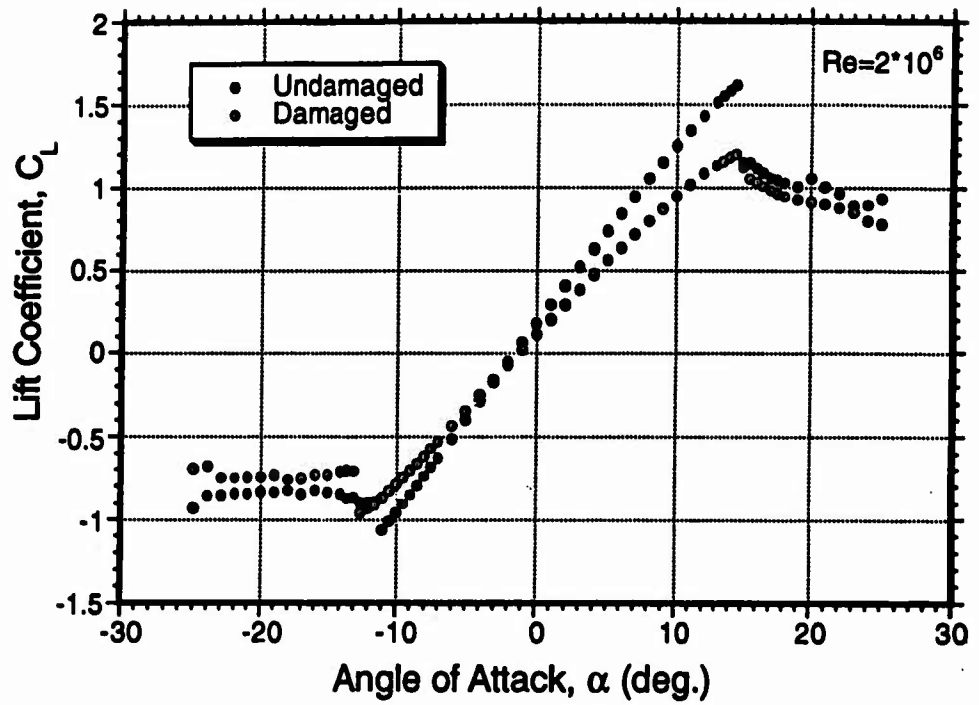
Figure 13: Lift Coefficient vs. Angle of Attack for Undamaged and Damaged Airfoils, $Re = 2 \times 10^6$.
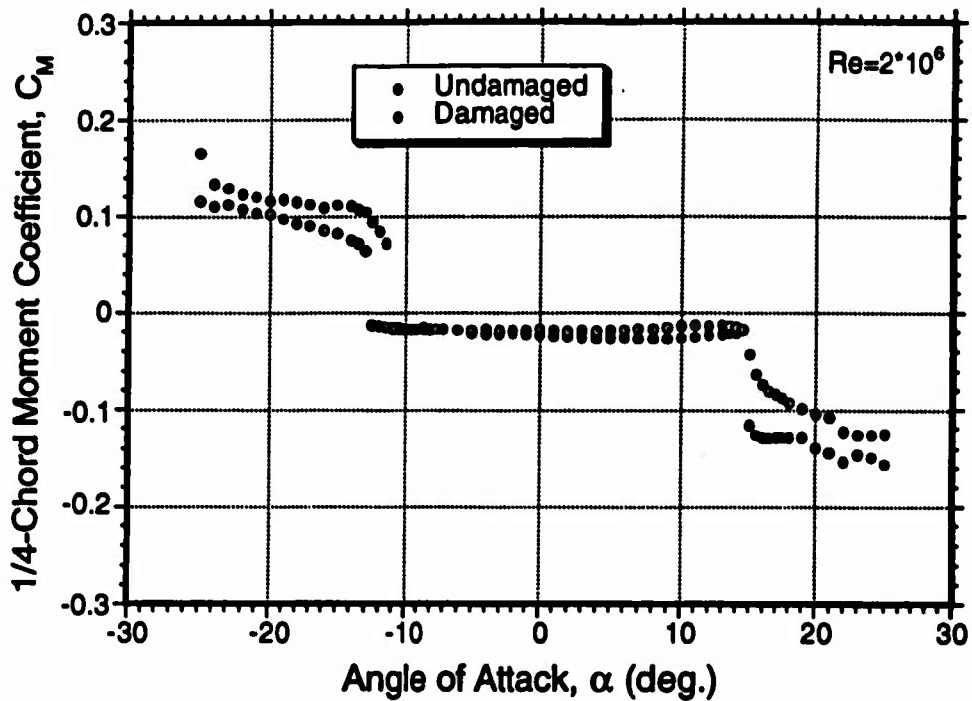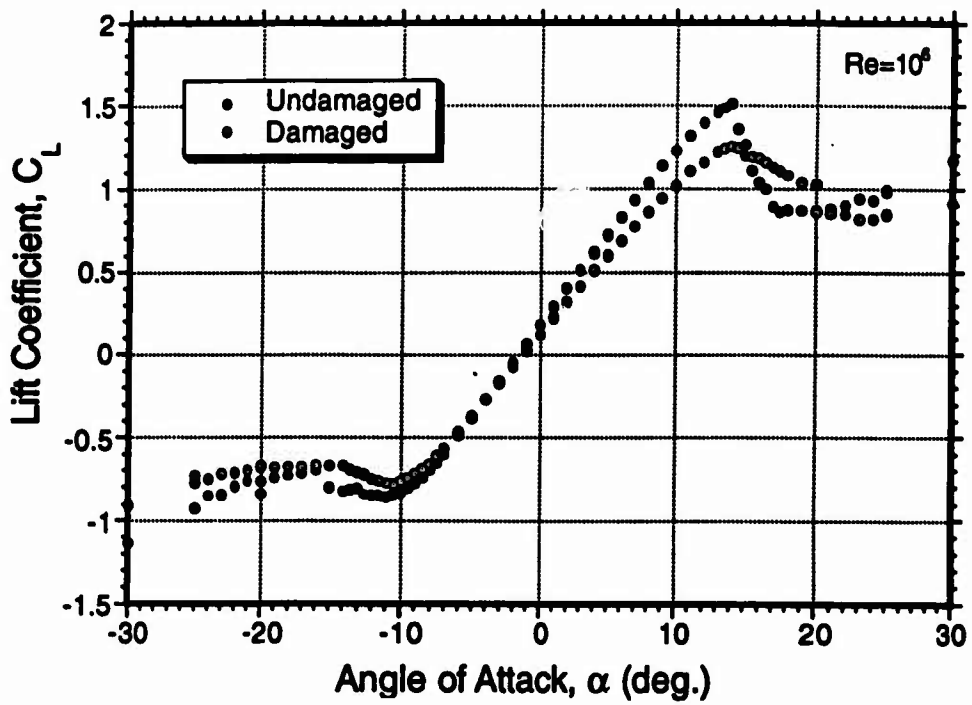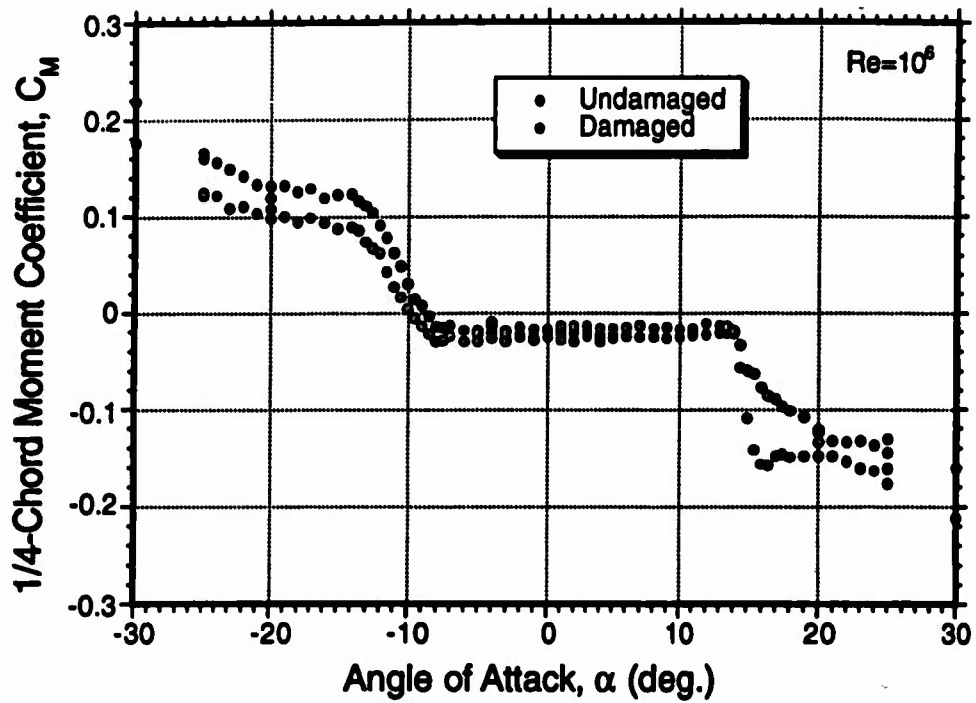
Figure 14: Moment Coefficient vs. Angle of Attack for Undamaged and Damaged Airfoils, $Re = 2 \times 10^6$.
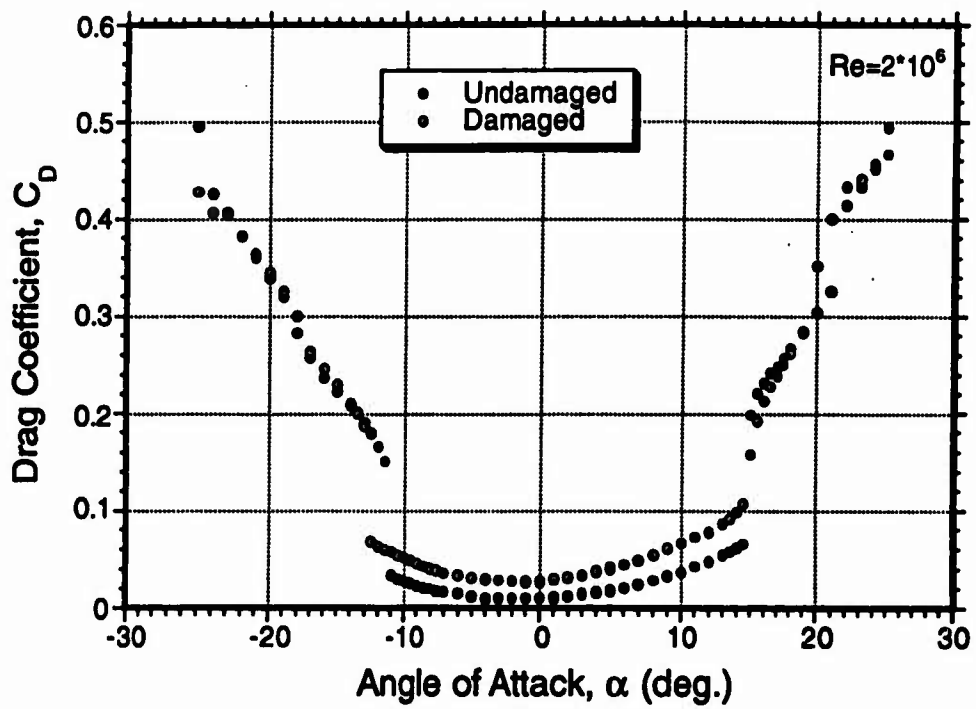
Figure 15: Drag Coefficient vs. Angle of Attack for Undamaged and Damaged Airfoils, $Re = 2 \times 10^6$.
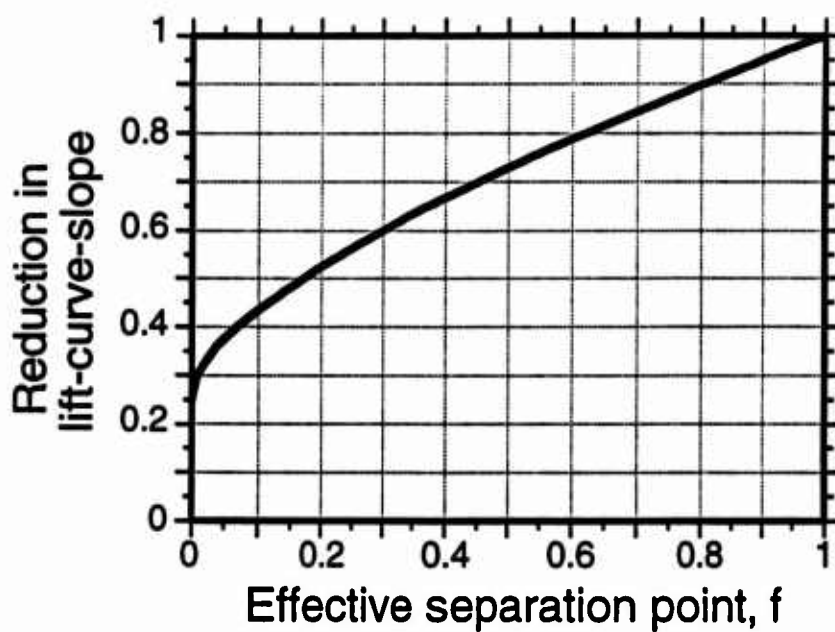
Figure 16: Reduction in Lift-Curve-Slope vs. Separation Point Using Kirchhoff Theory.
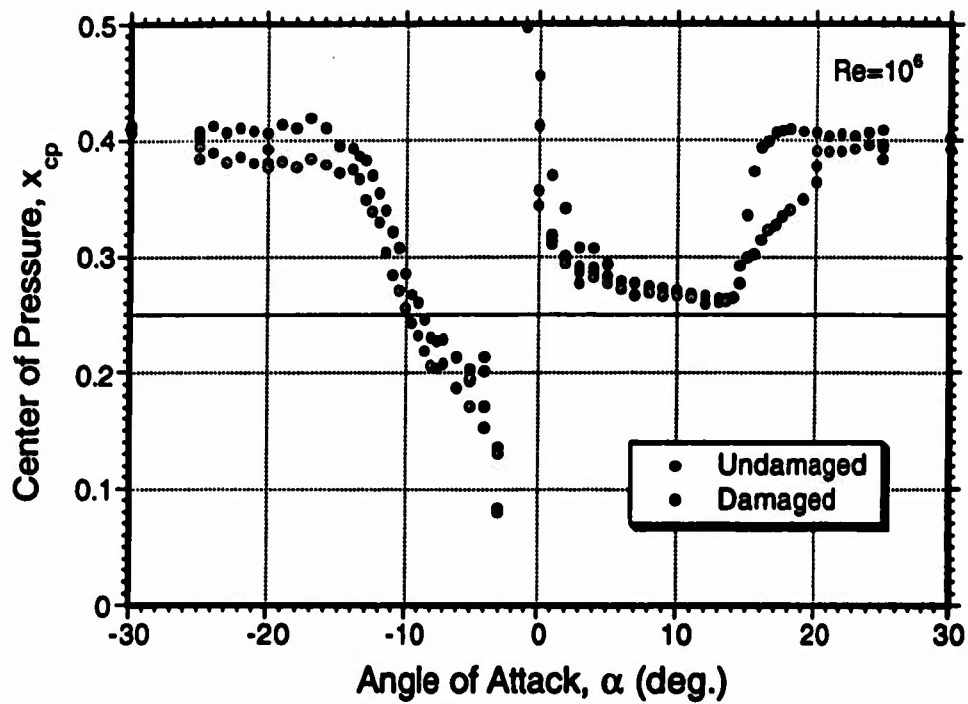
Figure 17: Variation in Center of Pressure for Undamaged and Damaged Airfoils, $Re = 10^6$.
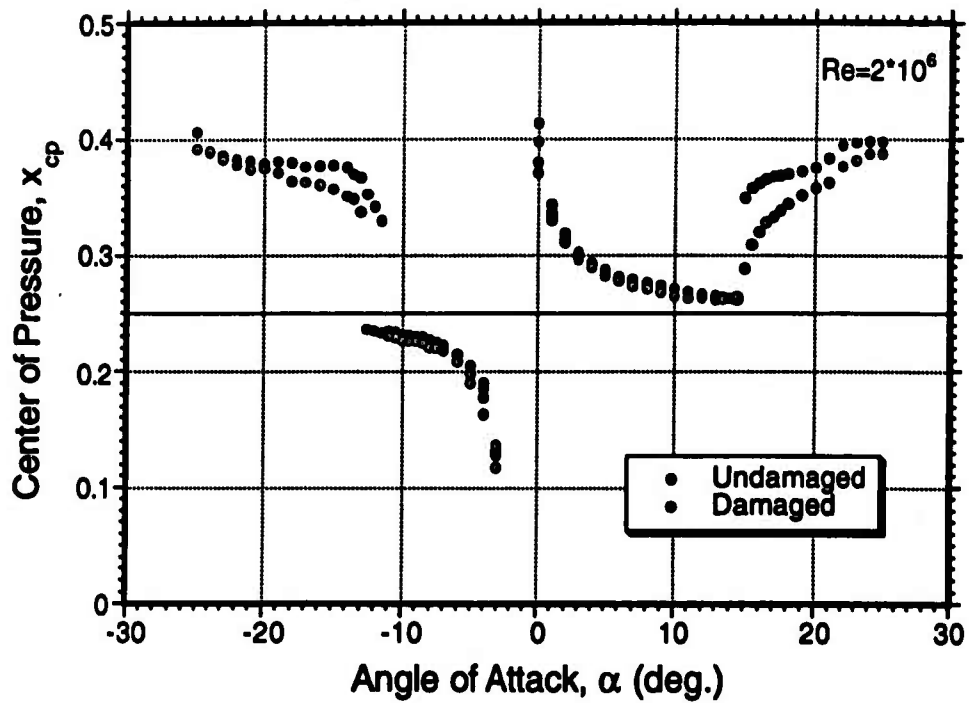
Figure 18: Variation in Center of Pressure for Undamaged and Damaged Airfoils, $Re = 2 \times 10^6$.
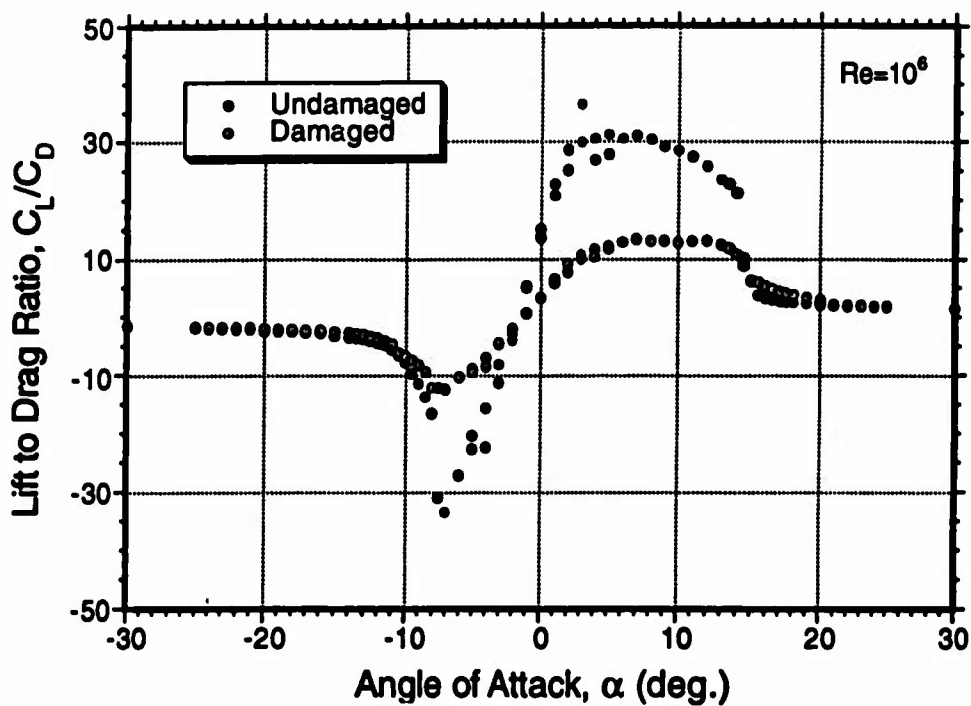
Figure 19: Lift to Drag Ratio vs. Angle of Attack for Undamaged and Damaged Airfoils, $Re = 10^6$.

Figure 20: Lift to Drag Ratio vs. Angle of Attack for Undamaged and Damaged Airfoils, $Re = 2 \times 10^6$.

Figure 21: Area Corrected Lift Coefficient vs. Angle of Attack for Damaged Airfoil, $Re = 10^6$.

Figure 22: Area Corrected Moment Coefficient vs. Angle of Attack for Damaged Airfoil, $Re = 10^6$.
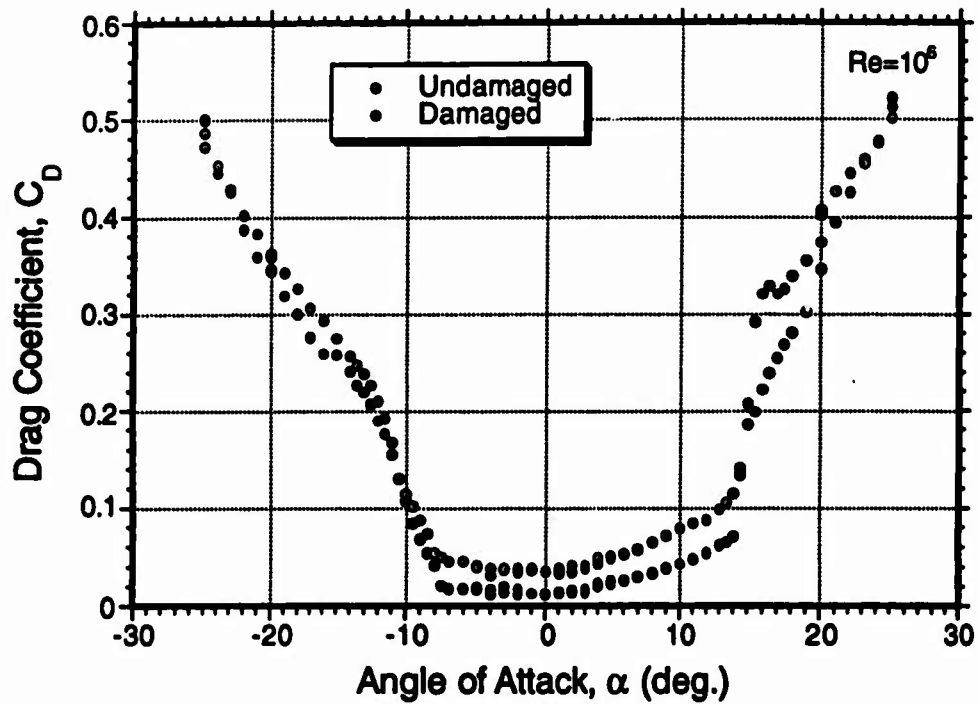
Figure 23: Area Corrected Drag Coefficient vs. Angle of Attack for Damaged Airfoil, $Re = 10^6$.
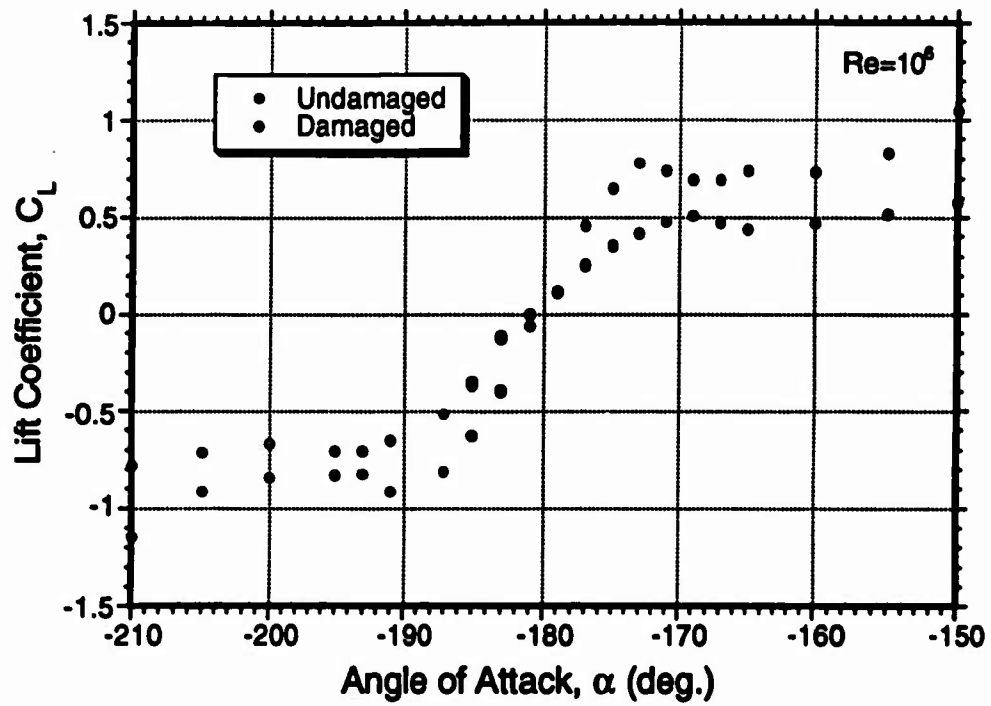
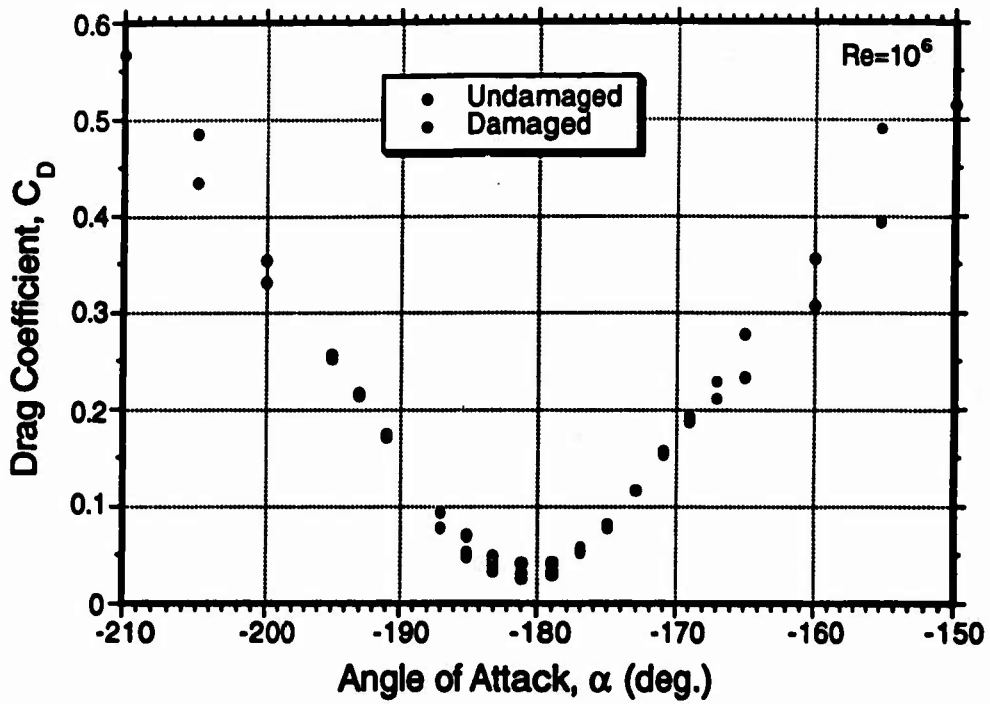Figure 24: Lift Coefficient in Reverse Flow for Undamaged and Damaged Airfoils, $Re = 10^6$.
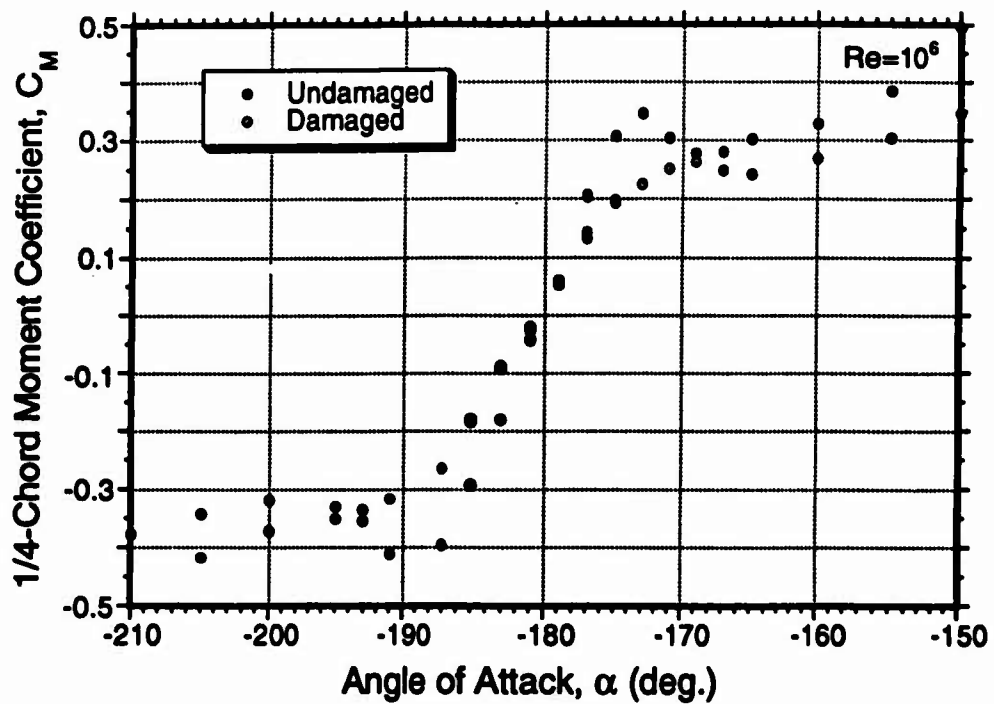
Figure 25: Moment Coefficient in Reverse Flow for Undamaged and Damaged Airfoils, $Re = 10^6$.

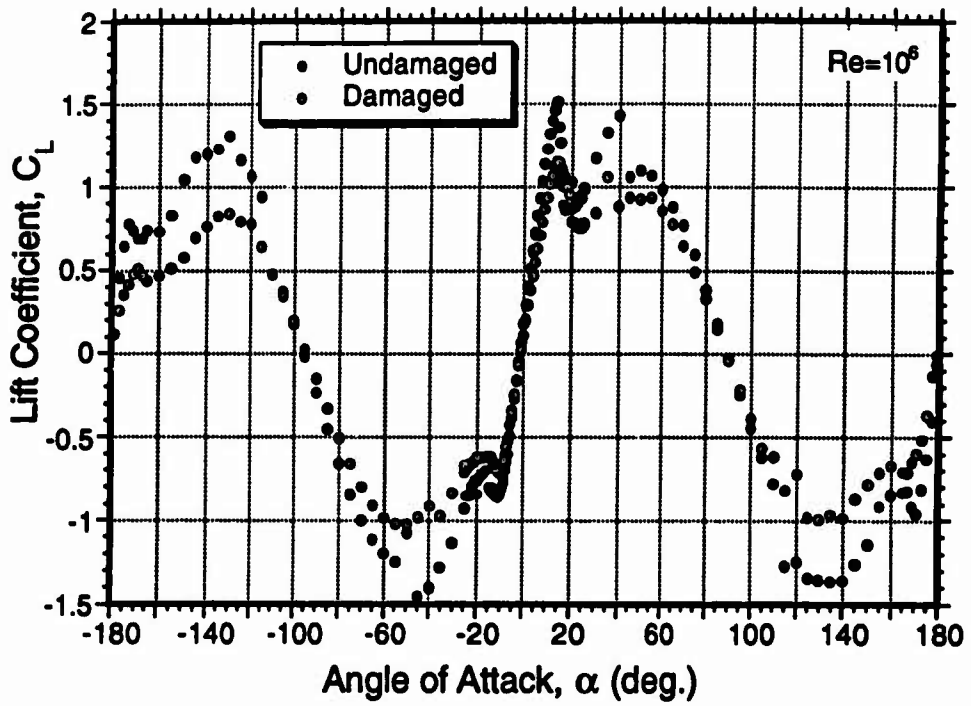Figure 26: Drag Coefficient in Reverse Flow for Undamaged and Damaged Airfoils, $Re = 10^6$.

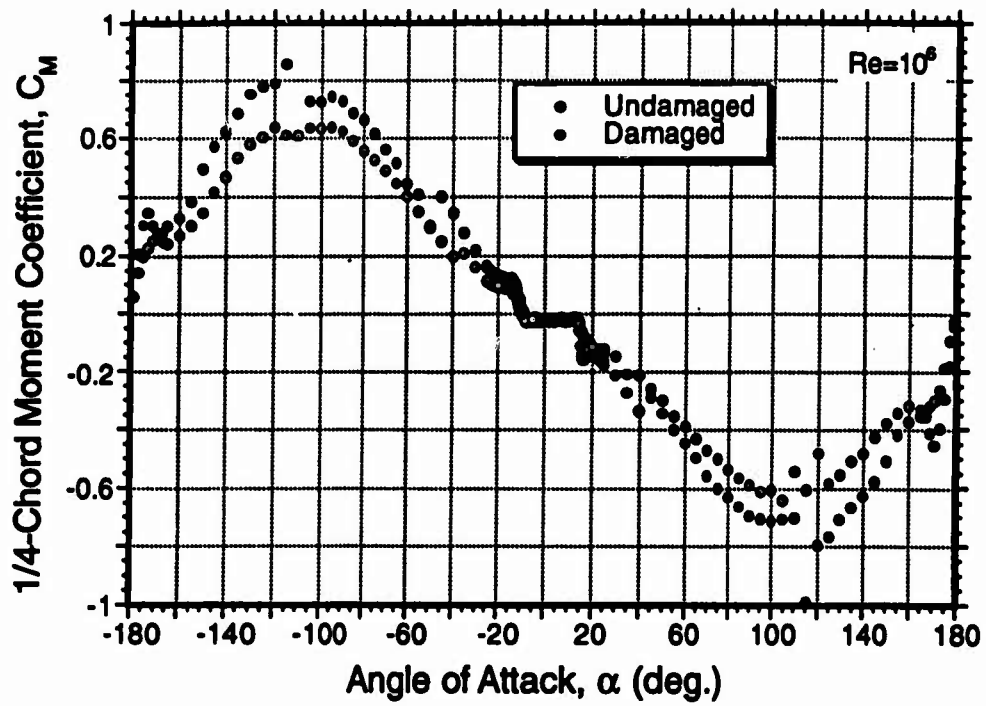Figure 27: Lift Coefficient in High Angles of Attack for Undamaged/Damaged Airfoils, $Re = 10^6$.

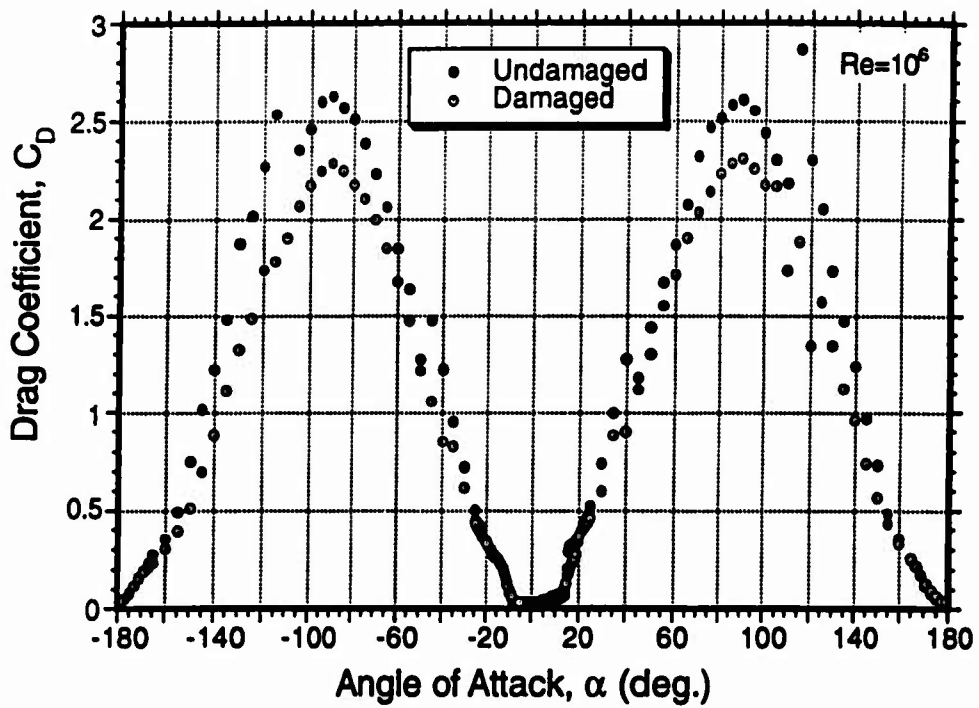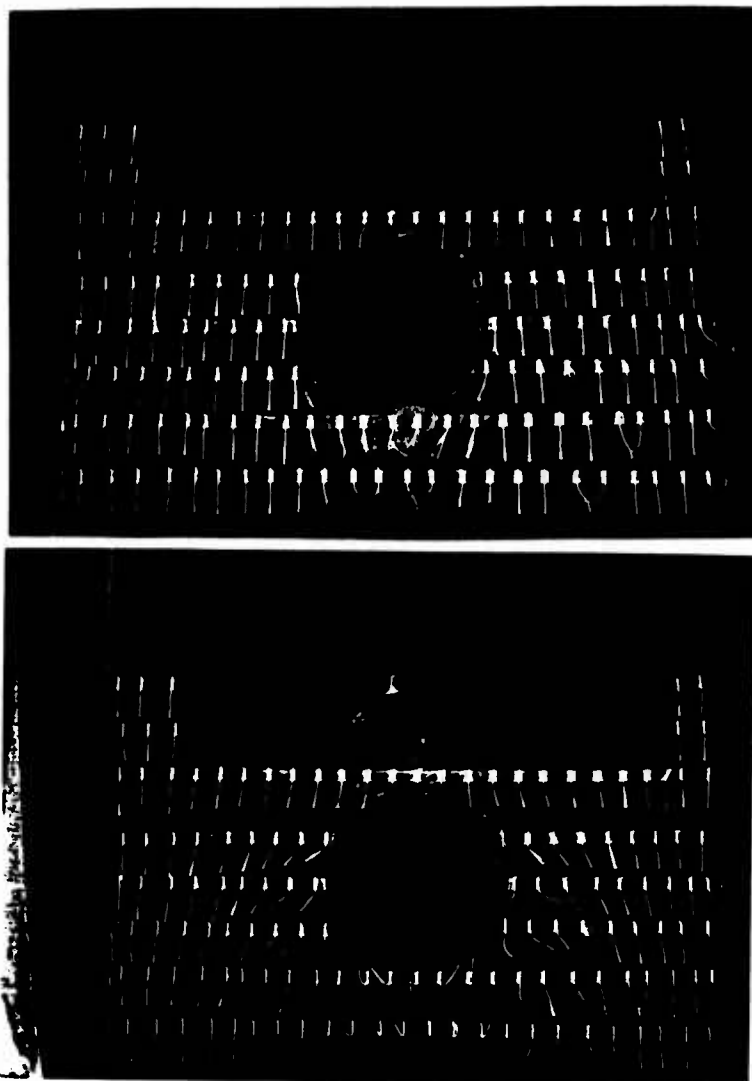Figure 28: Moment Coefficient in High Angles of Attack for Undamaged/Damaged Airfoils, $Re = 10^6$.

Figure 29:   Drag Coefficient in High Angles of Attack for Undamaged/Damaged Airfoils, $Re = 10^6$.

INCREASED ANGLE OF ATTACK

Figure 30: Mini-Tuft Flow Patterns on Wing with Simulated Ballistic Damage, $Re = 2 \times 10^6$.

Table 1: Summary of Test Runs.

Run No.	Re	Configuration	Model
1	Sweep	Calibration	Clean Tunnel
2	10^6	Pos. low angle sweep	Undamaged
3	10^6	Neg. low angle sweep	Undamaged
4	2×10^6	Pos. low angle sweep	Undamaged
5	2×10^6	Neg. low angle sweep	Undamaged
6	10^6	Pos. high angle sweep	Undamaged
7	10^6	Neg. high angle sweep	Undamaged
8	10^6	Pos. low angle sweep	Damaged
9	10^6	Neg. low angle sweep	Damaged
10	2×10^6	Pos. low angle sweep	Damaged
11	2×10^6	Neg. low angle sweep	Damaged
12	10^6	Tuft flow viz. video	Damaged
13	10^6	Pos. high angle sweep	Damaged
14	10^6	Neg. high angle sweep	Damaged
15	2×10^6	Tuft flow viz. still camera	Damaged

Table 2: Summary of Measured Characteristics for Undamaged (Reference) Airfoil.

Parameter	$Re = 10^6$	$Re = 2 \times 10^6$
Lift-curve-slope, C_{L_a}/deg.	0.1019	0.1057
Zero lift angle, α_0, deg.	-1.73	-1.64
Aerodynamic center, x_{ac}	0.2505	0.2517
Zero lift drag coefficient, C_{D_0}	0.01786	0.01296
$C_{L_{MAX}}$	1.51	1.62

Table 3: Comparison of Measured Characteristics for Undamaged and Damaged Airfoils.

Parameter	Undamaged $Re = 10^6$	Undamaged $Re = 2 \times 10^6$	Damaged $Re = 10^6$	Damaged $Re = 2 \times 10^6$
Lift-curve-slope, C_{L_α}/deg.	0.1019	0.1057	0.08406	0.08536
Zero lift angle, α_0, deg.	-1.73	-1.64	-1.28	-1.23
Aerodynamic center, x_{ac}	0.2505	0.2517	0.247	0.245
Zero lift drag coefficient, C_{D_0}	0.01786	0.01296	0.03619	0.03205
$C_{L_{MAX}}$	1.51	1.62	1.12	1.20

Table 4: Summary of Estimated Errors in Measured Quantities.

Parameter	Error
Lift, L	$\pm 0.1 \ lb_f$
Drag, D	$\pm 0.1 \ lb_f$
Moment, M	$\pm 0.5 \ in\text{-}lb_f$
Dynamic pressure, q_∞	$\pm 0.072 \ lb/ft^2$
Wing area, A	$0.013 \ ft^2$

V. References

1. Stephens, W., and M. Rutkowski *et al.* "Development of the Second Generation Comprehensive Helicopter Analysis System (2GCHAS)." *Proceedings of National Specialist's Meeting on Rotorcraft Dynamics.* Arlington, Texas, Nov. 1989.

2. Johnson, W. "A Comprehensive Analytical Model of Rotorcraft Aerodynamics and Dynamics, Part 1: Analysis Development." NASA TM-81182, NASA Ames Research Center, CA, June 1980.

3. Bir, G., I. Chopra, and K. C. Kim *et al.* "University of Maryland Advanced Rotorcraft Code (UMARC): Theory Manual." Technical Report, UMAERO-92-02, Center for Rotorcraft Research and Education, Univ. of Maryland, College Park, MD, 1992.

4. Yakowitz, S., and F. Szidarovszky. Introduction to Numerical Computation. New York, NY: Macmillan Publishing Co., 1989.

5. Woods, L. Theory of Subsonic Plane Flow. Cambridge, U.K.: Cambridge University Press, 1961.

INTENTIONALLY LEFT BLANK.

No. of Copies	Organization
3	Commander U.S. Army Aviation Systems Command ATTN: AMSAV-ESC, G. Kovacs SFAE-AV-BH-T, R. Olson SFAE-AV-AAH-SA, D. Roby 4300 Goodfellow Blvd. St. Louis, MO 63120-1798
2	Commander USAATCOM AATD ATTN: AMSAT-R-TF, G. Hufstetler SAVRT-TY-ASV, H. Reddick Ft. Eustis, VA 23604-5577
1	Commander AFSC HQ ASC ATTN: ASC/XRM, G. Bennett Wright-Patterson AFB, OH 45433-6503
1	Commander AFSC HQ WRDC ATTN: WL/FIVST, M. Lentz Wright-Patterson AFB, OH 45433-6553
1	Commander ATTN: ASC/XREWA, K. McArdle Eglin AFB, FL 32542-5600
2	Commander Dahlgren Division Naval Surface Warfare Center ATTN: Code G-13, T. Wasmund D. Dickinson Dahlgren, VA 22448
2	David Taylor Research Center Systems Department, Code 127 ATTN: Dr. David Haas Mr. John Vorwald Bethesda, MD 20084-5000
2	University of Maryland Dept. of Aerospace Engineering ATTN: Dr. J. G. Leishman Dr. J. Barlow College Park, MD 20742

No. of Copies	Organization
1	University of Texas at Arlington Aerospace Engineering ATTN: Dr. Shiv P. Joshi P.O. Box 19108 Arlington, TX 76019-0018
1	University of Kentucky Dept. of Engineering Mechanics ATTN: Dr. Susan W. Smith 467 Anderson Hall Lexington, KY 40506-0046
1	McDonnell Douglas Helicopter Company ATTN: William Sims 5000 E. McDowell Rd. Mesa, AZ 85205
1	Boeing Helicopters Division ATTN: N. Caravasos P.O. Box 16858 Philadelphia, PA 19142
1	Sikorsky Aircraft Mail Stop, Z101A ATTN: G. Burblis 6900 Main St. Stratford, CT 06601-1381

Aberdeen Proving Ground

No. of Copies	Organization
1	Dir, USAMSAA ATTN: AMXSY-AD, C. Alston
2	Dir, USARL ATTN: AMSRL-SL-B
47	Dir, USARL ATTN: AMSRL-SL-BA, K. Kim (40 cp) AMSRL-SL-I, Dr. Donald Haskell AMSRL-SL-BA, S. Polyak (5 cp) AMSRL-SL-N, M. Miller, Bldg. E3331

USER EVALUATION SHEET/CHANGE OF ADDRESS

This Laboratory undertakes a continuing effort to improve the quality of the reports it publishes. Your comments/answers to the items/questions below will aid us in our efforts.

1. ARL Report Number _____ **ARL-CR-66** _____ Date of Report _____ **September 1993** _____

2. Date Report Received _____

3. Does this report satisfy a need? (Comment on purpose, related project, or other area of interest for which the report will be used.) _____
_____
_____

4. Specifically, how is the report being used? (Information source, design data, procedure, source of ideas, etc.) _____
_____
_____

5. Has the information in this report led to any quantitative savings as far as man-hours or dollars saved, operating costs avoided, or efficiencies achieved, etc? If so, please elaborate. _____
_____
_____

6. General Comments. What do you think should be changed to improve future reports? (Indicate changes to organization, technical content, format, etc.) _____
_____
_____
_____

	_____
	Organization
CURRENT	_____
ADDRESS	Name
	_____
	Street or P.O. Box No.
	_____
	City, State, Zip Code

7. If indicating a Change of Address or Address Correction, please provide the Current or Correct address above and the Old or Incorrect address below.

	_____
	Organization
OLD	_____
ADDRESS	Name
	_____
	Street or P.O. Box No.
	_____
	City, State, Zip Code

(Remove this sheet, fold as indicated, tape closed, and mail.)
(DO NOT STAPLE)

BUSINESS REPLY MAIL
FIRST CLASS PERMIT No 0001, APG, MD

Postage will be paid by addressee.

Director
U.S. Army Research Laboratory
ATTN: AMSRL-OP-CI-B (Tech Lib)
Aberdeen Proving Ground, MD 21005-5066